Electron Capture in Charge-Tagged Peptides. Evidence for the Role of Excited Electronic States

Julia Chamot-Rooke, Christian Malosse, Gilles Frison, Frantisek Turecek

Electron Capture in Charge-Tagged Peptides. Evidence for the Role of Excited Electronic States

Julia Chamot-Rooke, Christian Malosse, Gilles Frison, and František Tureček*

Laboratoire des Mécanismes Réactionnels, Department of Chemistry, Ecole Polytechnique, CNRS, Palaiseau, France

Department of Chemistry, University of Washington, Seattle, WA 918195-1700, USA

Manuscript submitted to the *Journal of the American Society for Mass Spectrometry*, June 27, 2007

Revised manuscript submitted September 12, 2007

Running Title: Electron Capture in Charge-Tagged Peptides

Electron Capture in Charge-Tagged Peptides. Evidence for the Role of Excited Electronic States

Julia Chamot-Rooke, Christian Malosse, Gilles Frison, and František Tureček*

Laboratoire des Mécanismes Réactionnels, Department of Chemistry, Ecole Polytechnique, CNRS, Palaiseau, France

Department of Chemistry, University of Washington, Seattle, WA 918195-1700, USA

Abstract. Electron capture dissociation (ECD) was studied with doubly charged dipeptide ions that were tagged with fixed-charge tris-(2,4,6-trimethoxyphenyl)phosphonium-methylenecarboxamido (TMPP-ac) groups. Dipeptides GK, KG, AK, KA, and GR were each selectively tagged with one TMPP-ac group at the N-terminal amino group while the other charge was introduced by protonation at the lysine or arginine side-chain groups to give (TMPP-ac-peptide + H)$^{2+}$ ions by electrospray ionization. Doubly tagged peptide derivatives were also prepared from GK, KG, AK, and KA in which the fixed-charge TMPP-ac groups were attached to the N-terminal and lysine side-chain amino groups to give (TMPP-ac-peptide-ac-TMPP)$^{2+}$ dications by electrospray. ECD of (TMPP-ac-peptide + H)$^{2+}$ resulted in 72-84% conversion to singly charged dissociation products while no intact charge-reduced (TMPP-ac-dipeptide + H)$^{+\bullet}$ ions were detected. The dissociations involved loss of H, formation of (TMPP + H)$^{+}$, and N—C_α bond cleavages giving TMPP-$CH_2CONH_2^+$ ($\boldsymbol{c}_0$) and $\boldsymbol{c}_1$ fragments. In contrast, ECD of (TMPP-ac-peptide-ac-TMPP)$^{2+}$ resulted in 31-40% conversion to dissociation products due to loss of neutral TMPP molecules and 2,4,6-trimethoxyphenyl radicals. No peptide backbone cleavages were observed for the doubly tagged peptide ions. Ab initio and density functional

theory calculations for $(Ph_3P\text{-ac-GK} + H)^{2+}$ and $(H_3P\text{-ac-GK} + H)^{2+}$ analogs indicated that the doubly charged ions contained the lysine side-chain NH_3^+ group internally solvated by the COOH group. The distance between the charge-carrying phosphonium and ammonium atoms was calculated to be 13.1-13.2 Å in the most stable dication conformers. The intrinsic recombination energies of the $TMPP^+$-ac and $(GK + H)^+$ moieties, 2.7 and 3.15 eV, respectively, indicated that upon electron capture the ground electronic states of the $(TMPP\text{-ac-peptide} + H)^{+\bullet}$ ions retained the charge in the TMPP group. Ground electronic state $(TMPP\text{-ac-GK} + H)^{+\bullet}$ ions were calculated to spontaneously isomerize by lysine H-atom transfer to the COOH group to form dihydroxycarbinyl radical intermediates with the retention of the charged TMPP group. These can trigger cleavages of the adjacent N—C_α bonds to give rise to the $\boldsymbol{c}_1$ fragment ions. However, the calculated transition state energies for GK and GGK models suggested that the ground-state potential energy surface was not favorable for the formation of the abundant $\boldsymbol{c}_0$ fragment ions. This pointed to the involvement of excited electronic states according to the Utah-Washington mechanism of ECD.

Introduction

Electron-based methods of gas-phase ion chemistry rely on partial or complete neutralization of gas-phase ions to produce transient species with open electronic shells that undergo various dissociations [1]. Amongst the several electron-based methods in current use, electron capture dissociation (ECD)[2] has received much attention lately because of its potential for peptide and protein analysis [3]. ECD relies on dissociative recombination [4] with low-energy electrons of multiply charged, closed-shell, ions that are trapped in an ion-cyclotron resonance cell, followed by mass spectrometric analysis of the charged dissociation products. In parallel with the

analytical applications of ECD [5], there has been much interest in studying the dissociation mechanisms of cation-radicals produced by ion-electron recombination [6]. Experimental studies relied on peptide models in which the nature and sequence of amino acid residues were varied and the structure effects on ECD were interpreted on the basis of fragment ion analysis [6]. Computational studies of amide and small peptide models have addressed the electronic properties, dissociation, and transition state energies of open-shell intermediates that were suggested to play a role in ECD [7-10]. The crucial question in ECD concerns the site of electron attachment in the peptide ion that is thought to trigger bond dissociations. A possible electron attachment site is one of the charge-carrying groups, which in peptides are the protonated lysine, arginine, or histidine side-chain groups, the N-terminal amino group, or an amide group. Electron attachment in a protonated side-chain group (***X***, Scheme 1) produces a radical that may either dissociate or interact with the peptide backbone to transfer a hydrogen atom to the amide carbonyl through proton-coupled electron transfer [8]. Such a rearrangement would produce an aminoketyl radical intermediate which can be expected to readily undergo a β-fission dissociation [9]. Quantum theory calculations indicated that of several possible β-fission processes, N—C_α bond cleavages had the lowest activation energies [9,10] in keeping with the fact that N—C_α bond cleavages are regularly observed in ECD of peptide cations.

This so-called Cornell mechanism of ECD [11] has been scrutinized by studying the effects of electron attachment to basic side-chain groups in selected model systems, e.g., arginine amide [11], histidine N-methylamide [12], and β-alanine-N-methylamide [13], which had unequivocal protonation sites and well-defined conformations of gas-phase ions. The tendency for proton-coupled electron transfer to the amide groups decreases from ammonium (as in lysine and β-

alanine) through imidazolium (as in histidine) to guanidinium (as in arginine), which appears to be a poor hydrogen atom donor [11].

Another mechanism of ECD, called the Utah-Washington (UW) model [11], has been put forth to explain frequent dissociations of N—C_α bonds that for steric reasons may not be able to receive a hydrogen atom from the protonation sites of the precursor ions in their initial conformation(s) [14,15]. The UW model (Scheme 2) presumes competitive electron capture in amide π^* orbitals which are stabilized by electrostatic interaction with the remote charge-carrying groups. Electron capture dramatically changes the electronic properties of the amide group by substantially increasing its basicity (hence the amide superbase model) [14] while also lowering the N—C_α bond activation [14,15] and dissociation energy when compared to the same properties of a neutral amide group. Upon electron capture, the coulomb repulsion between the positively charged groups is compensated by attraction between the electron-carrying amide group and the remaining charge sites, and thus the charge-reduced intermediate can undergo conformational change followed by exothermic proton transfer (path ***a***) to form an aminoketyl intermediate that dissociates by N—C_α bond cleavage forming a $\boldsymbol{c}\ldots\boldsymbol{z}^{\bullet}$ fragment pair. Alternatively, the dissociation can follow path ***b*** in which the N—C_α bond cleavage and proton transfer steps are reversed. Note that the enol-imidate intermediate from N—C_α bond cleavage in path ***b*** is also highly basic and so we call it imine superbase in Scheme 2.

Distinction of the Cornell model on one hand and the alternative UW models on the other poses challenges in both experimental and computational approaches. On the experimental side, it is often difficult to control both the charge sites and ion conformations in gas-phase ions to provide well-defined reactant structures for reactivity studies. On the computational side, the multiply charged peptides used in ECD experiments are usually too big to allow for good quality

quantum theory calculations that would adequately represent the rather unusual electronic properties of peptide cation-radicals [8-14].

In the present work we attempt to bridge this gap between experiment and theory by studying ECD of doubly charged dipeptide ions that were furnished with a permanent charge at a fixed known position. As a charge-carrying group we chose tris-(2,4,6-trimethoxyphenyl)-phosphonium (TMPP) that can be selectively attached to amino groups at the peptide N-terminus or in the lysine side chain via a methylenecarboxamide linker [16]. Analogous TMPP derivatives have been used to introduce a fixed charge in larger peptides for ion dissociation [17] and ECD studies [18]. The other charge needed for ECD is introduced as a proton by electrospray ionization. The proton position is determined by the presence in the peptide of a single basic group, e.g., the lysine ε-amine, as in GK, KG, AK, and KA, or the arginine guanidine group as in GR. A potential advantage of these small dipeptide models is that the doubly charged gas-phase ions assume well-defined conformations due to Coulomb repulsion between the positive charges, which represents the dominant intramolecular interaction, and moreover, the gas-phase ion structures can be ascertained by quantum theory calculations. We also report ECD experiments with the same dipeptides containing two permanently charged TMPP groups. These derivatives do not possess mobile protons in the charged groups that would be needed to cause dissociations according to the Cornell model. We note that fixed-charge labeled peptides have also been used recently for studies of electron transfer dissociation [19].

Experimental Section

Materials. The peptides (Gly-Lys, Lys-Gly, Ala-Lys, Lys-Ala, and Gly-Arg) were obtained from Sigma-Aldrich and used without purification. Mono-TMPP derivatives were prepared by

mixing a peptide solution (1 nmol of peptide in 2 μL acetonitrile/water (2/8) (v/v) and 2 μL of 50 mM ammonium bicarbonate buffer (pH 8)) with 1 μL of 10 mM (N-succinimidyloxycarbonyl-methyl)-tris(2,4,6-trimethoxyphenyl)phosphonium bromide (Sigma-Aldrich). Under these conditions the more basic lysine amino group is protected by protonation and does not react. To introduce two TMPP groups, ammonium bicarbonate were replaced by 2 μL of 0.8-M N,N-diethylmethylamine that deprotonated the lysine ammonium group and rendered it reactive to the TMPP active ester reagent. The final solution was vortexed for 30 s and then sonicated in a water bath for 30 min (final bath temperature <30°C). The resulting mixture was evaporated (centrifugal evaporator) to dryness and the derivatives were stored at -20°C. Peptide solutions in acetonitrile/water/formic acid (49.5/49.5/1) at 2 to 20 μM concentrations were used for direct infusion using the electrospray ion source for the FT-ICR instrument and nanoelectrospray ion source for the QTOF mass spectrometer.

Methods. Electron capture dissociation mass spectra were obtained on a 7-T APEX III FT-ICR mass spectrometer (Bruker Daltonik, Bremen, Germany). Positive ions were produced by direct infusion of the peptide solutions into an external Apollo electrospray ion source (Bruker Daltonik) at a flow rate of 1.5 μL/min with the assistance of N_2 nebulizing gas. The ESI source parameters were: Cylinder, 0V; Capillary, -4000V; end plate, -3800V, cap exit, 50 V; skimmer 1, 16.4 V; skimmer 2, 7.1 V; offset, 0.3 V; trap and extract, 15 V and –10V respectively; drying temperature, 140°C. Ions were stored in the source region in a hexapole guide for 2 s and pulsed into the detection cell through a series of electrostatic lenses. Ions were finally trapped in the cell using gas–assisted dynamic trapping (Xe pulses, upper pressure around 10^{-7} mbar) with front and back trapping voltages of 3.0 and 3.5 V for trapping, reduced to 0.9 and 0.95 V for detection.

Ions of interest were isolated by radio frequency (rf) ejection of all unwanted ions using both low-voltage single rf pulses (soft shots) at their resonance frequencies and a chirp excitation covering the region of interest. ECD experiments were performed with an indirectly heated cathode operated at 1.9 A of heater current. Isolated doubly charged ions were irradiated during 300 ms with electrons having <1 eV kinetic energy. Mass spectra were acquired from *m*/*z* 200 to 2000 with 256 k data points and monoisotopic peaks were automatically labeled using the XMASS 6.1.4 (Bruker Daltonics) software.

Collision-induced dissociation (CID) mass spectra were obtained on a Q-Tof Premier™- (Waters Corp., Milford, MA, USA). The Q-Tof Premier™ is a quadrupole, orthogonal acceleration time-of-flight tandem mass spectrometer. Nanoelectrospray ionization in positive mode (ZSpray™) was used. Nano-electrospray glass capillaries (Proxeon, Denmark) were filled with 2 μl of the peptide solution and subsequently opened by breaking the tapered end of the tip under a microscope. The source temperature was set to 80 ºC. The capillary and cone voltages were set to 3000 and 40 V, respectively. The precursor ion selected in the first quadrupole was collisionally activated with argon using variable collision energy (10–45 eV for singly charged precursors and 5-20 eV for doubly charged parent ions). The TOF data were collected between *m*/*z* 100–1000. Scans were collected for 1 s and accumulated to increase the signal/noise ratio. Mass Lynx 4.1 was used both for acquisition and data processing. An external calibration in MS was done with clusters of phosphoric acid (0.01M in 50:50 acetonitrile:H_2O, v:v) before the analysis. The mass range for the calibration was *m/z* 70 - 2000.

Calculations. Standard ab initio calculations were performed using the Gaussian 03 suite of programs [20]. Optimized geometries were obtained by density functional theory calculations

using Becke's hybrid functional (B3LYP) [21] and the 6-31+G(d,p) basis set for dications and reoptimized with 6-31++G(d,p) for cation-radicals. The use of the 6-31++G(d,p) basis set was motivated by the need to incorporate diffuse functions on C, N, O, P, and H in calculations of hypervalent ammonium and phosphonium radicals and transition states for their dissociations and isomerizations. Hypervalent radicals have unpaired electrons in frontier molecular orbitals that resemble atomic Rydberg orbitals, 3s and 3p for N and 3d, 4s, 4p for P, which show substantial diffuse character, as studied previously for simple systems [22]. The optimized structures are shown in the pertinent schemes and figures. Complete optimized structures of all local minima and transition states can be obtained from the corresponding author upon request. Spin unrestricted calculations were performed for all open-shell systems. Stationary points were characterized by harmonic frequency calculations with B3LYP/6-31+G(d,p) as local minima (all real frequencies) and first-order saddle points (one imaginary frequency). The calculated frequencies were scaled with 0.963 [23] and used to obtain zero-point energy corrections, enthalpies, and entropies. The rigid-rotor-harmonic-oscillator (RRHO) model was used in thermochemical calculations except for low frequency modes where the vibrational enthalpy terms that exceeded 0.5 RT were replaced by free internal rotation terms equal to 0.5 RT.

Improved energies were obtained by single-point calculations using B3LYP and Møller-Plesset perturbation theory (MP2-frozen core) [24] that were carried out at several levels of theory, including the 6-311++G(2d,p) split-valence triple-ζ basis set furnished with polarization and diffuse functions. For the molecular systems studied here, the larger basis set comprised 648-1005 basis functions (968-1529 primitive gaussians). The spin unrestricted formalism was used for calculations of open-shell systems. Contamination by higher spin states was modest, as judged from the expectation values of the spin operator $\langle S^2 \rangle$ that were ≤0.76 for UB3LYP and

≤0.78 for UMP2 calculations. The UMP2 energies were corrected by spin annihilation [25] that reduced the $\langle S^2 \rangle$ to close to the theoretical value for a pure doublet state (0.75) after spin projection (PMP2). The B3LYP and MP2 energies calculated with the larger basis set were combined according to the B3-MP2 scheme, as described previously [26]. The largest molecular systems exceeded our computational resources for performing MP2 calculations, and for those only the B3LYP data are reported.

The performance of the B3-PMP2 scheme was checked by benchmark single-point calculations with coupled-cluster theory [27] including single, double, and disconnected triple excitations (CCSD(T)) [28] that were performed with the large correlation-consistent basis set of triple-ζ quality furnished with diffuse functions on all atoms, aug-cc-pVTZ [29]. The calculated recombination energies for PH_4^+ (eq 1) and dissociation energies for $PH_4^\bullet$ (eq 2) indicated that the B3-PMP2 scheme can be reliably used for phosphonium ions and radicals.

$$PH_4^+ + e^- \rightarrow PH_4^\bullet \qquad (1)$$

RE_{adiab} = –5.70 eV (B3-PMP2/6-311++G(2d,p)//B3LYP/6-311++G(2d,p))

RE_{adiab} = –5.70 eV (CCSD(T)/aug-cc-pVTZ//B3LYP/6-311++G(2d,p))

$$PH_4^\bullet \rightarrow PH_3 + H^\bullet \qquad (2)$$

$\Delta H^\circ_{g,0}$ = 16.9 kJ mol^{-1} (B3-PMP2/6-311++G(2d,p)//B3LYP/6-311+G(2d,p))

$\Delta H^\circ_{g,0}$ = 14.9 kJ mol^{-1} (CCSD(T)/aug-cc-pVTZ//B3LYP/6-311++G(2d,p))

Excited-state energies were calculated with time-dependent density functional theory [30] using the B3LYP functional and the 6-311++G(2d,p) basis set. Natural Population Analysis

(NPA)[31] was used to calculated atomic charges and spin densities with B3LYP/6-31++G(2d,p). Rice-Ramsperger-Kassel-Marcus (RRKM) theory was used to calculate unimolecular rate constants, as reported previously [13].

Results

ECD Spectra. Electron capture dissociations were studied with dications derived from singly TMPP-derivatized dipeptides that upon electrospray gave (TMPP-ac-peptide + H)$^{2+}$ ions containing one fixed triarylphosphonium charge and one protonation site. These ions are denoted as **1**$^{2+}$, **2**$^{2+}$, **3**$^{2+}$, **4**$^{2+}$, and **5**$^{2+}$ for GK, KG, AK, KA, and GR, respectively. Dications derived from doubly-derivatized peptides gave (TMPP-ac-peptide-ac-TMPP)$^{2+}$ ions containing two fixed-charge triarylphosphonium groups which are denoted as **6**$^{2+}$, **7**$^{2+}$, **8**$^{2+}$, and **9**$^{2+}$ for GK, KG, AK, and KA, respectively. The "ac" stands for the —CH_2CO— group linking the Ar_3P phosphonium group to the peptide amino group, according to the notation used by Watson et al. [16]. The peptide fragment ions are denoted by the standard letter symbols (***a*$_1$**, ***c*$_1$**, ***c*$_0$**, etc.) [32] where index 1 stands for cleavage between the amino acid residues and index 0 stands for bond cleavages at the TMPP linker amide group.

ECD of all peptide derivatives resulted in complete dissociation of the charge-reduced ions, and no cation-radicals corresponding to (TMPP-ac-peptide + H)$^{+\bullet}$ or (TMPP-ac-peptide-ac-TMPP)$^{+\bullet}$ were detected. ECD of the (TMPP-ac-peptide + H)$^{2+}$ dications showed substantial conversions to singly charged dissociation products, as defined by the formula: %conversion = $100\Sigma I_{ECD}/(\Sigma I_{ECD} + I_{precursor})$, which ranged within 79-84% for GK, KG, AK, and KA, and 72% for GR. The conversions in the (TMPP-ac-peptide-ac-TMPP)$^{2+}$ group were 31-40% or about half of those for the singly derivatized peptide dications.

The fragments formed from the (TMPP-ac-peptide + H)$^{+\bullet}$ intermediates were identified on the basis of accurate mass measurements and homologous mass shifts between Ala and Gly (Table 1). The ECD spectra are represented by those of (TMPP-ac-GK + H)$^{2+}$ (**1**$^{2+}$) and (TMPP-ac-KG + H)$^{2+}$ (**2**$^{2+}$) (Figure 1a,b). ECD of **1**$^{2+}$ produced ions at *m/z* 776 (loss of H), 746 (loss of H and CH_2O), 647 (***c*$_1$** fragment, loss of $C_6H_{12}NO_2$), 590 (***c*$_0$** fragment, $Ar_3P^+CH_2CONH_2$), 533 (Ar_3PH^+), and 501 $(Ar_3PH - CH_3OH)^+$. ECD of (TMPP-ac-AK + H)$^{2+}$ (**3**$^{2+}$) gave analogous and homologous fragments of the same type (Table 1). ECD of **2**$^{2+}$ produced ions at *m/z* 776 (loss of H), 746 (loss of H and CH_2O), 718 (***c*$_1$** fragment, loss of $C_3H_5O_2$), 590 (***c*$_0$** fragment, $Ar_3P^+CH_2CONH_2$), 573 (***c*$_0$** - NH_3), and 533 (Ar_3PH^+). ECD of (TMPP-ac-KA + H)$^{2+}$ (**4**$^{2+}$) gave analogous and homologous fragment ions of the same type (Table 1). Thus, the ECD spectra of all four singly derivatized peptides showed fragments formed by N—C_α cleavages at both amide groups. In addition, cleavage of the Ar_3P—CH_2 bond occurred that was accompanied by a proton transfer forming the most abundant Ar_3PH^+ cation.

The ECD mass spectrum of (TMPP-ac-GR + H)$^{2+}$ (**5**$^{2+}$) showed fragments at *m/z* 804 (loss of H), 717 (loss of $C_3H_{10}N_3$ from the Arg side chain), 647 (***c*$_1$** fragment, loss of $C_6H_{12}N_3O_2$), 638 (loss of trimethoxyphenyl radical), 590 (***c*$_0$**), 533 (Ar_3PH^+), and 470 (loss of CH_3OH + OCH_3 from Ar_3PH^+)(Figure 2).

The absence of charge reduced (TMPP-ac-peptide + H)$^{+\bullet}$ ions from GK, KG, AK, KA, and GR was consistent with the natural isotope abundances in the pertinent *m/z* 776-778 and 790-793 ion groups. For example, the [A + 1]/[A] abundance ratios [33] for [*m/z* 791]/[*m/z* 790] from AK and KA (measured as 0.392 and 0.374, respectively) were close to those in the doubly-charged precursors, [*m/z* 396]/[*m/z* 395.5] = 0.448 and 0.396 for AK and KA, respectively. The theoretical [A + 1]/[A] ratio for $C_{38}H_{54}N_3O_{13}P$ is 0.443. The data indicated that the contributions

of (TMPP-ac-peptide + H)$^{+\bullet}$ at the pertinent *m/z* values were negligible and the peaks could be assigned to the natural isotope satellites.

CID Spectra. In order to sort out electron-based and charge-driven dissociations upon electron capture, the ECD spectra were compared to collision-induced dissociation (CID) spectra of (TMPP-ac-peptide + H)$^{2+}$ and (TMPP-ac-peptide)$^{+}$ ions, as shown for GK and KG (Figure 3a,b). The CID spectrum of the (TMPP-ac-GK)$^{+}$ ion at *m/z* 776 (Figure 3a) showed a number of fragments that indicated extensive rearrangements upon collisional activation. Loss of the C-terminal amino acid (lysine $C_6H_{12}N_2O$) (*m/z* 648 and 662 for GK and AK, respectively), as well as formation of $\boldsymbol{a_1}$ ions (*m/z* 602 and 616 for GK and AK, respectively) were observed in the spectra. Both fragmentations have been previously reported for singly charged TMPP peptide derivatives [17]. The spectra also showed fragment ions originating from the $Ar_3P^+CH_2CONH$ moiety, e.g., $Ar_3PCH{=}C{=}O^+$ (*m/z* 573), *m/z* 527, 381, 351, and $ArPCH_2^+$ (*m/z* 181). The latter fragments are typical of triarylphosphonium ions, as reported previously [34].

CID of the (TMPP-ac-KG)$^{+}$ ion at *m/z* 776 (Figure 3b) showed elimination of a $C_8H_{14}N_2O_3$ fragment (*m/z* 590), and the above-listed arylphosphonium fragment ions. The CID spectra of the (TMPP-ac-peptide + H)$^{2+}$ ions showed essentially the same dissociations as did the (TMPP-ac-peptide)$^{+}$ ions but also involved proton-driven formation of lysine $\boldsymbol{y_1}$ ions.

The important conclusion from the comparison of the ECD and CID spectra was that they mostly contained different fragment ions and thus were mutually exclusive. We note that there is a coincidental overlap at *m/z* 590 due to the formation of the $Ar_3P^+CH_2CONH_2$ fragment ion by both charge-driven or charge-remote dissociation of (TMPP-ac-KG)$^{+}$ and (TMPP-ac-KA)$^{+}$ on the one hand, and electron-induced dissociation of (TMPP-ac-KG + H)$^{2+}$ and (TMPP-ac-KA +

H)$^{2+}$ on the other. Note, however, that ion dissociations of the (TMPP-ac-GK + H)$^{2+}$ and (TMPP-ac-AK + H)$^{2+}$ ions did not produce the *m/z* 590 fragment ions at all, and so their presence in the corresponding ECD spectra must be due to exclusive electron-induced dissociations. The relative intensities of the *m/z* 590 $\boldsymbol{c}_0$ ions, expressed as [$\boldsymbol{c_0}$]/[(TMPP-ac-peptide]$^+$ ratios, were greater for KG than for GK (1.7 and 0.5, respectively) and also for KA than AK (1.0 and 0.77 respectively), which indicated that a fraction of the *m/z* 590 fragment ions from KG and KA could be formed by consecutive dissociations of the primary (TMPP-ac-peptide)$^+$ fragments from ECD, as indicated by the pertinent CID spectra.

Derivatization of the lysine amino group in (TMPP-ac-peptide-ac-TMPP)$^{2+}$ had a substantial effect on the ECD mass spectra. As already mentioned, the presence of the second TMPP-ac group reduced the electron capture efficiency by a factor of two. Even more remarkably, ECD of (TMPP-ac-peptide-ac-TMPP)$^{2+}$ ions did not result in peptide backbone dissociations, as illustrated with the GK and KG-derived ions, **6**$^{2+}$ and **7**$^{2+}$, respectively (Figure 4a,b). Although the charge-reduced ions dissociated completely and no peaks of (TMPP-ac-peptide-ac-TMPP)$^{+\bullet}$ were detected at *m/z* 1349 for GK and KG, the observed fragments were due to loss of 2,4,6-trimethoxyphenyl radicals (*m/z* 1182) and the Ar_3P molecules (*m/z* 817) and consecutive dissociations of the latter primary fragment ions. Interesting is the elimination of a CH_3O radical from the *m/z* 817 ions which indicates internal cyclization by attack of the $^{\bullet}CH_2CO$-NH radical at one of the remaining 2,4,6-trimethoxyphenyl groups. The *m/z* 644 ions from **6**$^{2+}$, **7**$^{2+}$ and **9**$^{2+}$ may correspond to $Ar_3P^+CH_2CONHC_4H_7$ from the derivatized lysine side chain. The fragment ions at *m/z* 704 for **6**$^{2+}$ and**7**$^{2+}$ and *m/z* 718 for **9**$^{2+}$ are complementary by mass to *m/z* 644 and may correspond to the cleavage of the same C_α—C_β lysine bond with an inverse hydrogen transfer onto the neutral fragment. Note that *m/z* (644 + 704) = *m/z* 1348 which is the mass of the

whole GK or KG peptide minus H. The measured exact *m/z* ratios for ECD fragment ions from $\mathbf{6}^{2+}$-$\mathbf{9}^{2+}$ are summarized in Table 2.

Discussion

ECD of the singly-derivatized (TMPP-ac-peptide + H)$^{2+}$ ions showed competitive loss of a hydrogen atom, N—C_α bond cleavages at both amide groups, and P—C_α bond dissociation in the phosphonium moiety that was accompanied by a proton transfer. The loss of H probably occurred as a result of electron attachment to the lysine ammonium group, by analogy with dissociations of other ammonium radicals [22] and peptide models [8,13]. Interestingly, ECD of (TMPP-ac-peptide + H)$^{2+}$ ions did not promote elimination of ammonia, which is a common fragmentation upon ECD of non-derivatized peptide ions. Our observation is in line with the recent energy analysis of a peptide radical model which indicated that loss of ammonia from the side-chain ammonium group required a higher activation energy than did loss of an H atom, and so the former dissociation was disfavored [13]. In contrast, ECD-induced loss of ammonia is predicted to be extremely facile from protonated N-terminal ammonium groups [8] which are absent in the TMPP-derivatized peptides.

Ion Structures. To explain the dissociations of the N—C_α and P—C_α bonds we performed extensive quantum chemistry calculations of ion and radical structures, electronic states, and dissociation energies. Since the TMPP group is rather large ($C_{27}H_{33}O_9P$, 70 atoms) it was simulated by PH_3, triphenylphosphonium (TPP) and tris-(2,4,6-trihydroxyphenyl)phosphonium (THPP) groups that were presumed to have electronic properties converging to those of TMPP. The intrinsic properties of the dipeptide moiety were studied for (GK + H)$^\bullet$ and (GR + H)$^\bullet$

radicals. The interaction between the phosphonium and protonated dipeptide moieties was modeled in conjugates that had PH_3-CH_2CO- (structures $\mathbf{10a}^{2+}$-$\mathbf{10c}^{2+}$) or TPP-CH_2CO- groups (structures $\mathbf{11a}^{2+}$-$\mathbf{11c}^{2+}$) linked to the GK dipeptide (Figure 5).

The doubly charged ions $\mathbf{10}^{2+}$ and $\mathbf{11}^{2+}$ were each found to have more than one conformation corresponding to a local energy minimum. The lowest energy conformers $\mathbf{10a}^{2+}$ and $\mathbf{11a}^{2+}$ had the lysine side-chain NH_3^+ group hydrogen bonded to the carboxylate C-terminus. Higher-energy conformers $\mathbf{10b}^{2+}$ and $\mathbf{11b}^{2+}$ had the lysine side-chain NH_3^+ group hydrogen bonded to the Gly amide carbonyl. The calculated free energy difference, e.g., $\Delta G_{g,298}(\mathbf{10a}^{2+} \rightarrow \mathbf{10b}^{2+})$ = 32 kJ mol^{-1}, clearly preferred the carboxylate-solvated conformer, and the free energy difference further increased at higher temperatures, e.g., $\Delta G_{g,473}(\mathbf{10a}^{2+} \rightarrow \mathbf{10b}^{2+})$ = 33.6 kJ mol^{-1}, due to the lower entropy of $\mathbf{10b}^{2+}$. A conformer with a fully extended lysine side chain was also found to be a local energy minimum ($\mathbf{10c}^{2+}$, Figure 5). However structure $\mathbf{10c}^{2+}$ was less stable than $\mathbf{10a}^{2+}$, $\Delta G_{g,298}(\mathbf{10a}^{2+} \rightarrow \mathbf{10c}^{2+})$ = 14.4 kJ mol^{-1}, indicating that the stabilization gained by intramolecular hydrogen bonding in conformer $\mathbf{10a}^{2+}$ was more favorable than a decrease in Coulomb repulsion between the two charge sites in the more extended conformer $\mathbf{10c}^{2+}$. Lysine hydrogen bonding to the COOH group is also preferred in $\mathbf{11}^{2+}$, e.g., $\Delta G_{g,298}(\mathbf{11a}^{2+} \rightarrow \mathbf{11b}^{2+})$ = 20 kJ mol^{-1}, and $\Delta G_{g,298}(\mathbf{11a}^{2+} \rightarrow \mathbf{11c}^{2+})$ = 31 kJ mol^{-1}. Hence, we conclude that the calculated relative enthalpies and free energies for the model peptide conformers $\mathbf{10}^{2+}$ and $\mathbf{11}^{2+}$ indicated that the C-terminal lysine ammonium group was most likely hydrogen bonded to the carboxyl group, not the amide carbonyls, in the most stable and thus most populated conformers of the (TMPP-ac-peptide + H)$^{2+}$ dications $\mathbf{1}^{2+}$ and $\mathbf{3}^{2+}$. The calculated $\Delta G_{g,298}$ values give 99.7% of both $\mathbf{10a}^{2+}$ and $\mathbf{11a}^{2+}$ at equilibrium indicating substantial conformational homogeneity of the ion

populations. Lysine hydrogen bonding in $\mathbf{2}^{2+}$, $\mathbf{4}^{2+}$, and the arginine side chain H-bonding in $\mathbf{5}^{2+}$ were not studied here.

Are the structures of the charge-tagged peptide dications relevant for those of standard peptide ions? To address this question, we note that the distance between the charge-carrying phosphonium and ammonium atoms in the most stable conformers $\mathbf{10a}^{2+}$ and $\mathbf{11a}^{2+}$ (13.14 and 13.22 Å, respectively, Figure 5) is comparable to or greater than the distance between the charge carrying arginine guanidinium and lysine ammonium groups in doubly protonated Substance P (11.2-12.0 Å), as documented by fully optimized structures of the RPKP motif (Figure S1, Supplementary Material). Thus, the coulomb repulsion between the charge sites in $\mathbf{10a}^{2+}$ and $\mathbf{11a}^{2+}$ is of a similar magnitude as in standard peptide ions used for ECD studies.

Ion Recombination Energies. Electron attachment to the doubly charged ions depends on the intrinsic recombination energies (RE) of the charged sites to reach the ground electronic state of the charge-reduced cation-radical. Because the charged sites are remote in the dications, they affect each other mainly by through-space Coulomb effects which can be expressed by additive energy terms. We investigated the intrinsic group recombination energies in $(GK + H)^+$, $(GGK + H)^{2+}$, $(GR + H)^+$, THPP-$CH_2CONH_2^+$ and in a series of other phosphonium ions. The combined charge effects on the RE in the doubly charged ions were studied for $(PH_3CH_2CO\text{-}GK + H)^{2+}$.

The intrinsic recombination energies (absolute values) of phosphonium ions decrease upon addition of phenyl or 2,4,6-trihydroxyphenyl and alkyl groups to the phosphorus atom to reach $|RE_{adiab}| = 3.07$ eV in $Ar_3P^+CH_2CONH_2$ (Ar = 2,4,6-trihydroxyphenyl, THPP, Table 3). A further decrease by ca. 0.3 eV can be expected upon replacing the phenol hydroxy groups in THPP by methoxy groups in TMPP, by analogy with the 0.3 eV decrease in ionization energies

in methoxybenzenes when compared to those in phenols [34]. Hence, the intrinsic recombination energy of TMPP is estimated to be as low as $\left|RE_{adiab}\right| \approx 2.7$ eV.

The $Ar_3P^+CH_2CONH$ group underwent only minor structural changes upon electron attachment. The optimized structures of the THPP-CH_2CONH_2 cation (**12**$^+$) and radical (**12**$^\bullet$) are shown in Figure S2 (Supplementary Material). Both structures show essentially tetrahedral phosphorus atoms with a minor flattening of the C_1-C_2-C_4-P base which is due to steric repulsion of the aromatic rings. The P—CH_2 bond length practically did not change upon electron attachment whereas the P—C_1 aryl bond was extended by 0.073 Å in the radical (Figure S2). Note that tetravalent phosphoranyl radicals typically prefer trigonal bipyramidal geometries about the sp^3d hybridized P atom in which the odd-electron containing orbital assumes an equatorial or axial position [35]. Thus, the near-tetrahedral structure of **12**$^\bullet$ indicates that the electron is in a large part delocalized over the aromatic π-orbital system in triaryl phosphonium radicals.

The intrinsic recombination energy of the protonated GK moiety can be estimated from the calculated vertical RE as 3.15 eV. It is noteworthy that the $(GK + H)^\bullet$ radical formed by electron attachment to the $(GK + H)^+$ cation is not a local energy minimum, but it rearranges by an exothermic H atom migration to the COOH group to form a stable dihydroxycarbinyl radical (**13**$^\bullet$, Scheme 3). Thus, when including the change in energy due to the rearrangement, one obtains $\left|RE_{adiab}\right|(GK + H)^+ = 4.24$ eV (Table 3). The effect on the RE of the other charge can be estimated from the comparison of the vertical RE of $(GK + H)^+$ (3.15 eV) and **10a**$^{2+}$ (4.82) as $\Delta RE = 4.82 - 3.15 = 1.67$ eV. Again, the adiabatic RE of **10a**$^{2+}$ was less useful, because upon attachment the electron ended up in the PH_3 group in the ground electronic state of the cation-radical and caused substantial structure changes due to an $sp^3 \rightarrow sp^3d$ bond rehybridization

around the phosphorus atom. From the combined intrinsic recombination energies and charge effects we estimate the vertical recombination energies of $\mathbf{1}^{2+}$, $\mathbf{2}^{2+}$, $\mathbf{3}^{2+}$, and $\mathbf{4}^{2+}$ to be close to 3.15 + 1.67 = 4.82 eV when producing lysine ammonium radicals, whereas the charge remains in the Ar_3P group in the ground electronic state of the cation-radical.

In contrast, the vertical recombination energy of the $(GR + H)^+$ cation ($\mathbf{19}^+$, Scheme 4) was calculated as RE_{vert} = 2.81 eV for electron attachment to the guanidinium group. Hence, the intrinsic recombination energy of the guanidinium group was close to that of TMPP. This indicates that electron attachment to $(TMPP\text{-}ac\text{-}GR + H)^{2+}$ could occur in overlapping manifolds of near-degenerate states, one delocalized over the TMPP group and the other in the arginine guanidinium group. Note the large difference between the optimized cation and radical structure (Scheme 4) that results in large Franck-Condon effects in electron capture, as discussed later.

Discussion of Reaction Mechanisms. We now discuss the possible mechanisms for the formation of $\boldsymbol{c}_0$ and $\boldsymbol{c}_1$ fragments from the charge-tagged GK peptide ions. Application of the Cornell mechanism to ECD in $\mathbf{1}^{2+}$- $\mathbf{4}^{2+}$ would require hydrogen atom transfer from the protonated group to one of the amide carbonyls. However, the ion conformations indicate that the vast majority of GK dications have the charged lysine side chains internally solvated by the carboxylate, not amide groups. Can the ions rearrange their conformations during or after electron capture to enable a hydrogen transfer to the amide groups according to the Cornell mechanism?

We address this question by analyzing H-atom migrations following electron capture in simpler systems, e.g., $(GK + H)^+ + e^- \rightarrow (GK + H)^{\bullet}$ and $(GGK + 2H)^{2+} + e^- \rightarrow (GGK + 2H)^{+\bullet}$, that are amenable to good quality quantum theory calculations of their ground doublet electronic

states. The $(GK + H)^+$ cation (**13**$^+$, Scheme 3) has the lysine ammonium group internally solvated by the carboxyl group, as in the dominant conformers of charge-tagged ions **10**$^{2+}$ and **11**$^{2+}$. Upon electron attachment, the ground doublet electronic state of the incipient radical undergoes spontaneous barrierless rearrangement by H-atom migration to the carboxyl carbonyl forming the dihydroxycarbinyl radical **13**$^\bullet$. The fact that the incipient lysine ammonium radical is not a local energy minimum implies that it cannot undergo a conformational rearrangement to deliver the hydrogen atom to the amide group. Note that conformational changes in gas-phase ions and radicals require small yet finite activation energies on the order of 7-15 kJ mol^{-1} that limit the rate constants to ca. 10^{12} s^{-1}. In contrast, the H-atom migration forming **13**$^\bullet$ occurs on a repulsive potential energy surface within one N—H vibration (ν(N—H) = 2859 cm^{-1}), which limits the lifetime of the incipient ammonium radical to less than one vibrational period, $T = 1/(2\pi c\nu) = 2 \times 10^{-15}$ s. Hence, no kinetic process that has to overcome a finite energy barrier can compete with this barrierless isomerization.

We now describe that the spontaneous rearrangement upon electron attachment which moves the ammonium proton to the COOH group can trigger the formation of the $\boldsymbol{c}_1$ fragments through a relay-type mechanism [6b,6d] proceeding on the ground electronic state, as studied for (**13**$^\bullet$), and shown in Scheme 3 under the assumption that the presence of the remote charge in the triarylphosphonium group would represent only a minor perturbation of the radical system [14, see below]. Also shown in Scheme 3 are the radical relative energies in kJ mol^{-1} (values in parentheses).

The dihydroxycarbinyl radical (**13**$^\bullet$) produced by electron capture in **13**$^+$ can, in principle, undergo a β-fission of the N—C_α bond. However, a direct cleavage of this bond leads to an amidyl radical product (not shown in Scheme 3), which is a high-energy species. Energetically

more plausible pathways were found that involved practically thermoneutral conformational changes by which the HO-C-OH group rotated to become hydrogen bonded to the $\boldsymbol{c}_1$-amide carbonyl, as in intermediates **14**$^{\bullet}$ and **17**$^{\bullet}$ (Scheme 3). N—C_α bond cleavages in the latter radicals require only low TS energies in the pertinent transition states **TS1** and **TS3** to exothermically form dipole-dipole complexes **16**$^{\bullet}$ and **18**$^{\bullet}$, respectively, that can eventually dissociate to convergently form the $\boldsymbol{c}_1$ fragment.

Since the N—C_α bond dissociations in **14**$^{\bullet}$ and **17**$^{\bullet}$ are accompanied by proton migration to the incipient $\boldsymbol{c}_1$ fragments, a question arises if the hydrogen atom can migrate to the amide group in a relay-type step-wise mechanism to promote dissociation of an N—C_α bond that was initially remote from the radical site, e.g., in the formation of the $\boldsymbol{c}_0$ ions. This was studied with **14**$^{\bullet}$ for which we found a transition state (**TS2**) for H-atom transfer to the proximate amide carbonyl to give aminoketyl intermediate **15**$^{\bullet}$ (Scheme 3). However, the **TS2** energy was above those for **TS1** and **TS3** which kinetically disfavored the H-atom migration. This was corroborated by RRKM calculations (Figure S3, Supplementary Material) which showed that the N—C_α bond dissociations in **14**$^{\bullet}$ and **17**$^{\bullet}$ were 2.5-12 fold faster than the H-atom migration over a 50-350 kJ mol^{-1} range of radical internal energies.

H-atom migration to a more remote amide carbonyl in the presence of charge was studied for electron attachment to $(GGK + 2H)^{2+}$ cations **20**$^{+}$ and **21**$^{+}$ (Scheme 5). By analogy with **13**$^{\bullet}$, electron capture in the ground doublet state of **21**$^{\bullet}$ results in a barrierless H-atom migration to the COOH group forming the dihydroxycarbinyl cation radical **22**$^{+\bullet}$ in which the residual charge is located in the internally solvated N-terminal ammonium group. However, H-atom transfer onto the more remote amide carbonyl requires 90 kJ mol^{-1} in the transition state (**TS4**) and thus is even less favorable than a transfer to the neighboring amide group (**TS2**). One might note that

in addition to having an activation energy that exceeds those typically found for N—C_α bond dissociations [9,10], the H-atom migration from the dihydroxycarbinyl radical to a remote amide carbonyl would also be disfavored entropically.

The possible effect on the transition states for H-atom migration of the residual charge was studied for the extreme cases of no charge (as in **TS2**) and a very close charge (as in **TS4**, Scheme 5). NPA atomic charge densities at the recipient amide group were calculated for the reactants, transition states, and products. For the $\mathbf{14}^{\bullet} \rightarrow \mathbf{TS2} \rightarrow \mathbf{15}^{\bullet}$ migration, the charge in the recipient amide group goes from 0.41 in $\mathbf{14}^{\bullet}$ through 0.50 in **TS2** to -0.01 in $\mathbf{15}^{\bullet}$. This, while the product ($\mathbf{15}^{\bullet}$) could be expected to be stabilized in the presence of a remote positive charge at the N-terminus, stabilization of the transition state would be marginal. In the reaction $\mathbf{22}^{+\bullet} \rightarrow \mathbf{TS4}$, the charge in the N-terminal amide group goes from 0.09 to -0.52, indicating a polarizing effect of the proximate charge on the charge distribution in the transition state. In spite of this favorable effect, the transition state energy for the hydrogen migration is substantial, especially in comparison with the energetically much more favored N—C_α bond dissociations [9,10]. These model calculations strongly indicate that ground electronic states of charge-reduced ions may not have low-energy hydrogen migration pathways to produce intermediates that would allow for kinetically competitive bond cleavages at remote amide groups.

It may noted that while the hydrogen transfer from internally solvated lysine ammonium groups is spontaneous upon electron attachment, the guanidinium groups in arginine residues are poor H-atom donors and prefer other dissociation pathways [11]. Hence, the formation of the $\boldsymbol{c_1}$ fragment by the above-described relay mechanism may not be competitive in the GR peptide ions.

As discussed above, the formation of the $\boldsymbol{c}_0$ ions requires a cleavage of the N—C_α bond which is remote from both the lysine NH_3^+ group in the precursor dication and from the dihydroxycarbinyl radical site in the putative intermediates (e.g., **13**$^\bullet$), and thus this cleavage is difficult to rationalize by the same, relay-type, mechanism that was discussed above for the formation of the $\boldsymbol{c}_1$ ion. In keeping with the UW mechanism, one can presume that, in a fraction of dications, the electron enters a π* amide orbital corresponding to an excited electronic state of the charge-reduced ion. The electron in the π* state is stabilized by Coulomb interaction with the ammonium and phosphonium charges, e.g., structures **23** and **24** (Scheme 6). The reaction sequence in Scheme 6 involves a conformational change in **23** and **24** to bring the lysine ammonium or caboxyl groups to the negatively charged amidyl oxygens **(25**, **26**), followed by exothermic proton migration [8,13] forming the intermediate aminoketyl radicals **27** and **28**. The latter are expected to readily dissociate by N—C_α bond cleavage [9,10] giving ions $\boldsymbol{c}_\mathbf{0}$ and $\boldsymbol{c}_1$, respectively. It should be noted that the UW mechanism depicted in Scheme 6 still lacks on several details that are the subject of current investigations. For example, electron attachment to the particular π* amide orbital can be mediated by transfer through orbitals in one or more intermediate excited electronic states, and the cross sections for such electron transfer are unknown [15a,b]. Furthermore, the conformational properties of excited electronic states are difficult to investigate even for simple peptide models [15c], and so information on such potential energy surfaces is currently lacking.

Figure 6 shows the electronic states of the charge-reduced analog **10a**$^{+\bullet}$. The lowest electronic states (***X***, ***A***, and ***B***) correspond to the positive and negative combinations of the phosphonium 4s and ammonium 3s Rydberg-like orbitals in combination with a π* orbital of the COOH group. The nodal properties of the frontier molecular orbitals in the ***X***, ***A***, and ***B*** states are

favorable for a transfer of the ammonium proton onto the COOH group, which is barrier-less when the electron is attached to the ammonium group and can move to COOH by proton-coupled electron transfer [36]. In contrast, the low-lying ***C***, ***D***, and ***E*** states at 0.32, 0.50 and 0.70 eV excitation energies show substantial electron density in the relevant P-CH_2CO-NH amide group that can trigger its further reactions according to the UW mechanism. Note that the UW mechanism can also be used to explain the formation of the $\boldsymbol{c}_1$ ion. Electron capture in the charge-stabilized ***G*** state of a 0.93 eV excitation energy produces a reactive intermediate that after conformational change of the lysine chain can undergo exothermic proton transfer forming aminoketyl radical **23**. An N—C_α bond cleavage in the latter then gives ion $\boldsymbol{c}_1$.

Excited electronic states can be used to explain the formation of the abundant Ar_3PH^+ ions (*m/z* 533) which requires a dissociation of the P—C_α bond which is promoted by electron attachment to the phosphonium ion [35]. The recombination energy of the Ar_3P^+ group in $\mathbf{1}^{2+}$ and $\mathbf{3}^{2+}$ is estimated to be composed of its intrinsic RE (2.7 eV) and the coulomb term (1.67 eV) to give $\left| RE_{adiab} \right| \approx 4.4$ eV, which is ca. 0.4-0.5 eV above the ground state of the charge-reduced cation radical.

The molecular orbitals of the electronic states corresponding to electron capture in the Ar_3P group were modeled using the THPP-CH_2CONH_2 radical (Figure S4, Supplementary Material). The low-lying excited states show extensive delocalization of electron density by interaction of phosphorus 3d, 4s, and 4p orbitals with the π^* and σ^* orbitals of the aryl substituents. Cleavage of the P—CH_2CONH_2 bond in the radical was calculated to be 29-32 kJ mol^{-1} *exothermic* and required a low activation energy, e.g., E_{TS} = 4 kJ mol^{-1} in TPP$^\bullet CH_2CONH_2$. However, in the ECD experiments the incipient TMPP and $^\bullet CH_2$CONH-GK^+ fragments do not separate immediately after the P—C_α bond cleavage, as evidenced by the absence of the $^\bullet CH_2$CONH-

dipeptide^{+} cation-radicals at *m/z* 245 for GK and KG, *m/z* 259 for AK and KA, and *m/z* 273 for GR. As suggested in Scheme 6, the fragments remain temporarily engaged in an ion-molecule complex to allow proton transfer to occur. Interestingly, the calculated 298 K gas-phase basicity of tris-(2,4,6-trihydroxyphenyl)phosphine (GB_{298} = 1064 kJ mol^{-1}), which represents a lower limit for the GB of the more electron-rich TMPP, exceeds the gas phase basicity of Gly-Lys that was estimated at 934-953 kJ mol^{-1} by previous measurements [37], and is also above the gas-phase basicity of arginine (992 kJ mol^{-1})[37]. Thus, proton transfer to Ar_3P from the $^{\bullet}CH_2CONH$-peptide^{+} fragment is exothermic for both lysine and arginine. We note that the incipient Ar_3P fragment is spatially remote from the protonated lysine or arginine side chains in the reactants $\mathbf{1}^{+\bullet}$ - $\mathbf{5}^{+\bullet}$, as well as in the transition state for the P—C_α bond cleavage. The fact that *quantitative* proton transfer to Ar_3P occurs, as dictated by the reaction thermochemistry, is evidence that the incipient fragments interact in an ion-molecule complex before separation.

Doubly Tagged and Arginine Peptide Ions. We now discuss the electron-induced dissociations of the doubly TMPP-labeled peptide ions $\mathbf{6}^{2+}$-$\mathbf{9}^{2+}$ and the (TMPP-ac-GR)$^{2+}$ ion $\mathbf{5}^{2+}$. Ions $\mathbf{6}^{2+}$-$\mathbf{9}^{2+}$ completely dissociate by fragmentations within the TMPP moieties, but do not undergo backbone N—C_α bond cleavages. This behavior is different from the dissociations of larger peptides that were charge-tagged with trimethylalkylammonium groups [19] and did undergo regular N—C_α cleavages. This indicates that the electronic structure of the fixed-charge group and its interactions with the π^* orbitals of the peptide amide groups are important for the dissociations upon electron capture. The lack of N—C_α bond dissociations in $\mathbf{6}^{2+}$-$\mathbf{9}^{2+}$ indicates that electron attachment in the peptide orbitals that could trigger dissociations is inefficient. This may be due to the high density of electronic states within the TMPP groups (Figure S4) that

promote C—P bond dissociations while disfavoring electron transfer to the reactive π* amide orbitals.

Ion $\mathbf{5}^{2+}$ contains a guanidinium group which is an inefficient hydrogen atom donor in arginine radicals when formed in their ground electronic state [11]. However, the guanidinium group can exothermically transfer a proton to a reduced carboxyl or amide group in an excited electronic state, according to the UW mechanism (see above). It is noteworthy that the ground electronic state of a guanidinium radical with its puckered geometry poorly matches the planar guanidinium cation [11] and disfavors electron attachment in the guanidinium because of an unfavorable Franck-Condon overlap. Thus, electron capture in the π* carboxyl and amide orbitals can be particularly efficient in arginine containing peptides.

Also noteworthy is the presence of the *m/z* 638 peak in the ECD spectrum of $\mathbf{5}^{2+}$ which is due to the elimination of a 2,4,6-trimethoxyphenyl group from TMPP. As discussed for $\mathbf{6}^{2+}$-$\mathbf{9}^{2+}$, this dissociation is triggered by electron capture in the TMPP group. The fact that it occurs in $\mathbf{5}^{2+}$ is consistent with the low vertical recombination energy of the protonated guanidine group (2.81 eV), so that the electronic state manifolds of the guanidinium and TMPP radicals overlap. Furthermore, loss of a neutral guanidine molecule from $\mathbf{5}^{2+}$ (*m/z* 746) is negligible (Figure 2), in contrast to ECD of arginine-containing peptides where it represents a major low-energy dissociation pathway [11]. Its absence in ECD of $\mathbf{5}^{2+}$ indicates that the electron reaches the electronic states of the guanidine moiety in a negligible small fraction of charge-reduced ions. This may be due to a difference in the density of electronic and vibrational states at the TMPP and guanidinium groups in the incipient cation radical. The TMPP group shows only small changes of geometry upon electron capture (cf. Figure S2). In contrast, the relaxed geometries of the guanidinium ion and radical are different (Scheme 4) causing large Franck-Condon effects in

electron attachment [11], which decrease the density of states for electron capture at the guanidinium group. Given the similarity of the recombination energies of TMPP and guanidinium ions, the probability for electron attachment can be largely determined by the local density of states to favor capture at the TMPP group.

Conclusions

Electron-capture dissociation of charge-tagged GK, KG, AK, KA, and GR dipeptide dications showed strong dependence on the charge type. Backbone N—C_α bond cleavages were observed only in the presence of lysine ammonium or arginine guanidinium groups. In the absence of the charged peptide groups the ions dissociated by P—C bond cleavages in the triarylphosphonium groups. These results can be interpreted by a combination of a relay-type mechanism operating on the ground electronic-state potential energy surface and the Utah-Washington mechanism involving π^* amide orbitals in low-lying excited electronic states and accompanied by proton transfer. The relative importance of these two mechanisms cannot be determined from the current experiments. The fact that the N—C_α bond cleavages occur in the presence of arginine which is an inefficient hydrogen atom donor indicates that the UW mechanism may predominate.

Acknowledgements. F. T. thanks the National Science Foundation for support through Grants CHE-0349595 for experiments and CHE-0342956 for computations, and the Laboratory of Reaction Mechanisms at Ecole Polytechnique, Palaiseau, France, for a visiting fellowship in September 2006. J. C. R. thanks Emilie Biteau for some ECD experiments and G. van der Rest for fruitful discussions.

Supplementary Material: Figures S1-S4.

References

[1] Tureček, F. Transient Intermediates of Chemical Reactions by Neutralization-Reionization Mass Spectrometry. *Top. Curr. Chem.* **2003**, *225*, 77-129.

[2] Zubarev, R. A.; Kelleher, N. L.; McLafferty, F. W. Electron Capture Dissociation of Multiply Charged Protein Cations. A Nonergodic Process. *J. Am. Chem. Soc.* **1998**, *120*, 3265-3266.

[3] Zubarev, R. A.; Horn, D. M.; Fridriksson, E. K.; Kelleher, N. L.; Kruger, N. A.; Lewis, M. A.; Carpenter, B. K.; McLafferty, F. W. Electron Capture Dissociation for Structural Characterization of Multiply Charged Protein Cations. *Anal. Chem.* **2000**, *72*, 563-573.

[4] Rowe, B. R.; Mitchell, J. B.; Canosa, A (Eds.) *Dissociative Recombination. Theory, Experiment, and Applications*, Plenum Press: New York, 1993.

[5] Cooper, H. J.; Hakansson, K.; Marshall, A. G. The role of electron capture dissociation in biomolecular analysis. *Mass Spectrom. Rev.* **2005**, *24*, 201-222.

[6] (a) Zubarev, R. A.; Horn, D. M.; Fridriksson, E. K.; Kelleher, N. L.; Kruger, N. A.; Lewis, M. A.;Carpenter, B. K.; McLafferty, F. W. *Anal. Chem.* **2000,** *72*, 563-573. (b) Leymarie, N.; Costello, C. E.; O'Connor, P. B. Electron Capture Dissociation Initiates a Free Radical Reaction Cascade. *J. Am. Chem. Soc.* **2003**, *125*, 8949-8958. (c) Fung, Y. M. E.; Chan, T.-W. D. Experimental and Theoretical Investigations of the Loss of Amino Acid Side Chains in Electron Capture Dissociation of Model Peptides. *J. Am. Soc. Mass Spectrom.* **2005**, *16*, 1523-1535. (d) O'Connor, P. B.; Lin, C.; Cournoyer, J. J.; Pittman, J. L.; Belyayev, M.; Budnik, B. A. Long-Lived Electron Capture Dissociation Product Ions Experience Radical Migration via Hydrogen Abstraction. *J. Am. Soc. Mass Spectrom.* **2006**, *17*, 576-585. (e) Lin, C.; Cournoyer, J. J.; O'Connor, P. B. Use of a Double Resonance Electron Capture

Dissociation Experiment to Probe Fragment Intermediate Lifetimes. *J. Am. Soc. Mass Spectrom.* **2006**, *17*, 1605-1615.

[7] (a) Konishi, H.; Yokotake, Y.; Ishibashi, T. Theoretical Study on the Electron Capture Dissociation Correlated with Proton Transfer Processes. *J. Mass Spectrom. Soc. Jpn.* **2002**, *50*, 222-225. (b) Bakken, V.; Helgaker, T.; Uggerud, E. Models of fragmentations induced by electron attachment to protonated peptides. *Eur. J. Mass Spectrom.* **2004**, *10*, 625-638.

[8] Tureček, F.; Syrstad, E. A. Mechanism and Energetics of Intramolecular Hydrogen Transfer Atom Transfer in Amide and Peptide Radicals and Cation-Radicals *J. Am. Chem. Soc.* **2003**, *125*, 3353-3369.

[9] Tureček, F. N—C_α Bond Dissociation Energies and Kinetics in Amide and Peptide Radicals. Is the Dissociation a Non-Ergodic Process? *J. Am. Chem. Soc.* **2003**, *125*, 5954-5963.

[10] Tureček, F.; Syrstad, E.A.; Seymour, J. L.; Chen, X.; Yao, C. Peptide Cation-Radicals. A Computational Study of the Competition between Peptide N—C_α Bond Cleavage and Loss of the Side Chain in the $[GlyPhe\text{-}NH_2 + 2H]^{+\bullet}$ Cation Radical. *J. Mass Spectrom.* **2003**, *38*, 1093-1104.

[11] Chen. X.; Tureček, F. The Arginine Anomaly. Arginine Radicals Are Poor Hydrogen Atom Donors in Electron Transfer Induced Dissociations. *J. Am. Chem. Soc.* **2006**, *128*, 12520-12530.

[12] Yao, C.; Fung, Y. M. E.; Tureček, F. Histidine Radicals. Presented at the UPPCON IV Conference, Hong Kong, December 2006.

[13] Yao, C.; Syrstad, E. A.; Tureček, F. Electron Transfer to Protonated β-Alanine N-Methylamide in the Gas Phase: An Experimental and Computational Study of Dissociation Energetics and Mechanisms. *J. Phys. Chem. A*, **2007**, *111*, 4167-4180.

[14] Syrstad, E. A.; Tureček, F. Toward a general mechanism of electron capture dissociation. *J. Am. Soc. Mass Spectrom.* **2005**, *16*, 208-224.

[15] (a) Sobczyk, M.; Anusiewicz, I.; Berdys-Kochanska, J.; Sawicka, A.; Skurski, P.; Simons, J. Coulomb-Assisted Dissociative Electron Attachment: Application to a Model Peptide. *J. Phys. Chem. A* **2005**, *109*, 250-258. (b) Anusiewicz, I.; Berdys-Kochanska, J.; Skurski, P.; Simons, J. Simulating Electron Transfer Attachment to a Positively Charged Model Peptide. *J. Phys. Chem. A* **2006**, *110*, 1261-1266. (c) Skurski, P.; Sobczyk, M.; Jakowski, J.; Simons, J. Possible mechanisms for protecting N—C_α bonds in helical peptides from electron capture (or transfer) dissociation. *Int. J. Mass Spectrom.* **2007**, *265*, 197-212.

[16] Huang, Z.-H.; Wu, J.; Roth, K. D. W.; Yang, Y.; Gage, D. A.; Watson, J. T. A Picomole-Scale Method for Charge Derivatization of Peptides for Sequence Analysis by Mass Spectrometry. *Anal. Chem.* **1997**, *69*, 137-144.

[17] Sadagopan, N.; Watson, J. T. Investigation of the Tris(trimethoxyphenyl)phosphonium Acetyl Charge Derivatives of Peptides by Electrospray Ionization Mass Spectrometry and Tandem Mass Spectrometry. *J. Am. Soc. Mass Spectrom.* **1999**, *11*, 107-119.

[18] Chamot-Rooke, J; van der Rest, G.; Dalleu, A.; Bay, A.; Lemoine, J. The Combination of Electron Capture Dissociation and Fixed Charge Derivatization Increases Sequence Coverage for OGlycosylated and O-Phosphorylated Peptides. *J. Am. Soc. Mass Spectrom.* **2007**, *18*, 1405-1413.

[19] Gunawardena, H. P.; Gorenstein, L.; Erickson, D. E.; Xia, Y.; McLuckey, S. A. Electron transfer dissociation of multiply protonated and fixed charge disulfide linked polypeptides. *Int. J. Mass Spectrom.* **2007**, *265*, 130-138.

[20] Frisch, M. J.; Trucks, G. W.; Schlegel, H. B.; Scuseria, G. E.; Robb, M. A.; Cheeseman, J. R.; Montgomery, J. A. , Jr.; Vreven, T.; Kudin, K. N.; Burant, J. C.; Millam, J. M.; Iyengar, S. S.; Tomasi, J.; Barone, V.; Mennucci, B.; Cossi, M.; Scalmani, G.; Rega, N.; Petersson, G. A.; Nakatsuji, H.; Hada, M.; Ehara, M.; Toyota, K.; Fukuda, R.; Hasegawa, J.; Ishida, M.; Nakajima, T.; Honda, Y.; Kitao, O.; Nakai, H.; Klene, M.; Li, X.; Knox, J. E.; Hratchian, H. P.; Cross, J. B.; Adamo, C.; Jaramillo, J.; Gomperts, R.; Stratmann, R. E.; Yazyev, O.; Austn, A. J.; Cammi, R.; Pomelli, C.; Ochterski, J., W.; Ayala, P. Y.; Morokuma, K.; Voth, G. A.; Salvador, P.; Dannenberg, J. J.; Zakrzewski, V. G.; Dapprich, S.; Daniels, A. D.; Strain, M. C.; Farkas, O.; Malick, D. K.; Rabuck, A. D.; Raghavachari, K.; Foresman, J. B.; Ortiz, J. V.; Cui, Q.; Baboul, A. G.; Clifford, S.; Cioslowski, J.; Stefanov, B. B.; Liu, G.; Liashenko, A.; Piskorz, P.; Komaromi, I.; Martin, R. L.; Fox, D. J.; Keith, T.; Al-Laham, M. A.; Peng, C. Y.; Nanayakkara, A.; Challacombe, M.; Gill, P. M. W.; Johnson, B.; Chen, W.; Wong, M. W.; Gonzalez, C.; Pople, J. A. *Gaussian 03, Revision B.05*; Gaussian, Inc.; Pittsburgh PA, 2003.

[21] (a) Becke, A. D. A New Mixing of Hartree-Fock and Local Density-Functional Theories. *J. Chem. Phys.* **1993**, *98*, 1372-1377. (b) Becke, A. D. Density Functional Thermochemistry. III. The Role of Exact Exchange. *J. Chem. Phys.* **1993**, *98*, 5648-5652.

[22] Yao, C.; Tureček, F. Hypervalent Ammonium Radicals. Competitive N—C and N—H Bond Dissociations in Methylammonium and Ethylammonium. *Phys. Chem. Chem. Phys.* **2005**, 7, 912-920.

[23] Rauhut, G.; Pulay, P. Transferable Scaling Factors for Density Functional Derived Vibrational Force Fields. *J. Phys. Chem.* **1995**, *99*, 3093-3100.

[24] Møller, C.; Plesset, M. S. A Note on an Approximation Treatment for Many-Electron Systems. *Phys. Rev.* **1934**, *46*, 618-622.

[25] (a) Schlegel, H. B. Potential Energy Curves Using Unrestricted Moller-Plesset Perturbation Theory with Spin Annihilation. *J. Chem. Phys.* **1986**, *84*, 4530-4534. (b) Mayer, I. Spin-Projected UHF Method. IV. Comparison of Potential Curves Given by Different One-Electron Methods. *Adv. Quantum Chem.* **1980**, *12*, 189-262.

[26] (a) Tureček, F. Proton Affinity of Dimethyl Sulfoxide and Relative Stabilities of C_2H_6OS Molecules and $C_2H_7OS^+$ Ions. A Comparative G2(MP2) ab Initio and Density Functional Theory Study. *J. Phys. Chem. A*, **1998**, *102*, 4703-4713. (b) Tureček, F.; Wolken, J. K. Dissociation Energies and Kinetics of Aminopyrimidinium Radicals by Ab Initio and Density Functional Theory. *J. Phys. Chem. A*, **1999**, *103*, 1905-1912. (c) Tureček, F.; Polášek, M.; Frank, A. J.; Sadílek, M. Transient Hydrogen Atom Adducts to Disulfides. Formation and Energetics. *J. Am. Chem. Soc.* **2000**, *122*, 2361-2370. (d) Polášek, M.; Tureček, F. Hydrogen Atom Adducts to Nitrobenzene. Formation of the Phenylnitronic Radical in the Gas Phase and Energetics of Wheland Intermediates. *J. Am. Chem. Soc.* **2000**, *122*, 9511-9524. (e) Rablen, P. R. Is the Acetate Anion Stabilized by Resonance or Electrostatics? A Systematic Structural Comparison. *J. Am. Chem. Soc.* **2000**, *122*, 357-368. (f) Rablen, P. R. Computational Analysis of the Solvent Effect on the Barrier to Rotation about the Conjugated C-N Bond in Methyl N,N-Dimethylcarbamate. *J. Org. Chem.* **2000**, *65*, 7930-7937. (g) Rablen, P. R.; Bentrup, K. H. Are the Enolates of Amides and Esters Stabilized by Electrostatics? *J. Am. Chem. Soc.* **2003**, *125*, 2142-2147. (h) Hirama, M.; Tokosumi, T.; Ishida, T.; Aihara, J. Possible molecular hydrogen formation mediated by the inner and outer carbon atoms of typical PAH cations *Chem. Phys.* **2004**, *305*, 307-316.

[27] Čížek, J.; Paldus, J.; Šroubková, L. Cluster Expansion Analysis for Delocalized Systems. *Int. J. Quantum Chem.* **1969**, *3*, 149-167.

[28] Purvis, G. D., III; Bartlett, R. J. A Full Coupled-Cluster Singles and Doubles model: The Inclusion of Disconnected Triples. *J. Chem. Phys.* **1982**, *76*, 1910-1918.

[29] (a) Dunning, T. H., Jr. Gaussian Basis Sets for Use in Correlated Molecular Calculations. I. The Atoms Boron through Neon and Hydrogen. *J. Chem. Phys.* **1989**, *90*, 1007-1023. (b) Woon, D. E.; Dunning, T. H., Jr. Gaussian Basis Sets for Use in Correlated Molecular Calculations. III. The Atoms Aluminum through Argon. *J. Chem. Phys.* **1993**, *98*, 1358-1371.

[30] Stratmann, R. E.; Scuseria, G. E.; Frisch, M. J. An Efficient Implementation of Time-Dependent Density Functional Theory for the Calculation of Excitation Energies of Large Molecules. *J. Chem. Phys.* **1998**, *109*, 8218-8224.

[31] Reed, A. E.; Weinstock, R. B.; Weinhold, F. Natural population analysis. *J. Chem. Phys.* **1985**, *83*, 735-746.

[32] (a) Roepstorff, P.; Fohlman, J. Proposal for a common nomenclature for sequence ions in mass spectra of peptides. *Biomed. Mass Spectrom.* **1984**, *11*, 601. (b) Johnson, R. S.; Martin, S. A.; Biemann, K. Collision-induced fragmentation of $(M + H)^+$ ions of peptides. Side chain specific sequence ions. *Int. J. Mass Spectrom. Ion Processes* **1988**, *86*, 137-54.

[33] McLafferty, F. W.; Tureček, F. Interpreation of Mass Spectra, 4th Ed.; University Science Books; Mill Valley, CA, 1993.

[34] Clareboudt, J.; Baten, W.; Geise, H.; Claeys M. Structural Characterization of Mono- and Biphosphonium Salts by Fast Atom Bombardment Mass Spectrometry and Tandem Mass Spectormetry. *Org. Mass Spectrom.* **1993**, *28*, 71-82.

[34] NIST Standard Reference Database Number 69, June 2005 Release, http://webbook.nist.gov/chemistry.

[35] (a) Gustafson, S. M.; Cramer, C. J. Ab Initio Conformational and Stereopermutational Analyses of Phosphoranyl Radicals HP(OR)3 and P(OR)4 [R = H or CH3]. *J. Phys. Chem.* **1995**, *99*, 2267-2277. (b) Tureček, F.; Gu, M.; Hop. C. E. C. A. Franck-Condon Dominated Chemistry. Formation and Dissociations of Tetrahydroxyphosphoranyl Radicals Following Femtosecond Reduction of Their Cations in the Gas Phase. *J. Phys. Chem.* **1995**, *99*, 2278-2291. (c) Cramer, C. J. The fluorophosphoranyl series: theoretical insights into relative stabilities and localization of spin. *J. Am.Chem. Soc.* **1991**, *113*, 2439-2447. (d) Cramer, C. J. Computational studies of open-shell phosphorus oxy acids. Pt. 3. Theoretical rotation, pseudorotation, and pseudoinversion barriers for the hydroxyphosphoranyl radical. *J. Am. Chem. Soc.* **1990**, *112*, 7965-7972.

[36] (a) Siegbahn, P .E. M.; Blomberg, M. R. A.; Crabtree, R. H. Hydrogen transfer in the presence of amino acid radicals. *Theor. Chem. Acc.* **1997**, *97*, 289-300. (b) Siegbahn, P. E. M.; Eriksson, L.; Himo, F.; Pavlov, M. Hydrogen Atom Transfer in Ribonucleotide Reductase (RNR). *J. Phys. Chem. B* **1998**, *102*, 10622-10629. (c) Cujier, R. L.; Nocera, D. G. Proton-Coupled Electron Transfer. *Annu. Rev. Phys. Chem.* **1998**, *49*, 337-369.

[37] Harrison, A. G. The gas-phase basicities and proton affinities of amino acids and peptides. *Mass Spectrom. Rev.* **1997**, *16*, 201-217.

Figure Captions

Figure 1. Electron-capture dissociation mass spectra of (a) (TMPP-ac-GK + H)$^{2+}$ (**1**$^{2+}$) and (b) (TMPP-ac-KG + H)$^{2+}$ (**2**$^{2+}$) precursor ions at *m/z* 388.6618. Noise peaks are marked with asterisks

Figure 2. ECD spectrum of (TMPP-ac-GR + H)$^{2+}$ (**5**$^{2+}$) at *m/z* 402.6648.

Figure 3. Collision-induced dissociation mass spectra of (a) (TMPP-ac-GK)$^{+}$ and (b) (TMPP-ac-KG)$^{+}$ ions at m/z 776.33.

Figure 4. Electron-capture dissociation mass spectra of (a) (TMPP-ac-GK-ac-TMPP)$^{2+}$ (**6**$^{2+}$) and (b) (TMPP-ac-KG-ac-TMPP)$^{2+}$ (**7**$^{2+}$) precursor ions at *m/z* 674.742. Noise peaks are marked with asterisks

Figure 5. B3LYP/6-31+G(d,p) optimized structures of ion conformers **10a**$^{2+}$-**10c**$^{2+}$, and **11a**$^{2+}$-**11c**$^{2+}$. Double arrows indicate intramolecular hydrogen bonds in angstroms.

Figure 6. Electronic states and vertical excitation energies in **10a**$^{+\bullet}$ from TD-B3LYP/6-311++G(2d,p) calculations.

Table 1. ECD Spectra of (TMPP-ac-peptide + H)$^{2+}$ Ions.

	Peptide				
Ion[a]	GK	KG	AK	KA	GR
(TMPP-ac-peptide + H)$^{2+}$	**1**$^{2+}$ 388.6618 *388.6619*[a]	**2**$^{2+}$ 388.6618	**3**$^{2+}$ 395.6696 *395.6697*	**4**$^{2+}$ 395.6695	**5**$^{2+}$ 402.6648 *402.665*
(TMPP-ac-peptide + H)$^{+\bullet}$	-	-	-	-	-
(TMPP-ac-peptide)$^{+}$	776.3153 *776.3159*	776.3153	790.3313 *790.3316*	790.3249	804.3211 *804.322*
(TMPP-ac-peptide)$^{+}$ - CH_2O	-	746.3065 *746.3053*	-	760.3086 *760.3181*	-
$\boldsymbol{c}_1$	647.2368 *647.2479*	718.3099 *718.3105*	661.2531 *661.2548*	718.3116 *718.3105*	647.2372 *647.237*
Loss of $C_9H_{11}O_3$	-	-	-	-	638.2598 *638.259*
$\boldsymbol{c}_1 - NH_3$	-	-	-	701.2868 *701.2839*	-
TMPP-ac-NH_2 ($\boldsymbol{c}_0$)	590.2154 *590.2197*	590.2157	590.2156	590.2169	590.2164
TMPP-$NH_2 - NH_3$	-	-	-	573.1905 *573.1963*	-
Ar_3PH[b]	533.1947 *533.1941*	533.1946	533.1943	533.1947	533.1946
$Ar_3PH^{+} - CH_3OH$	501.1693 *501.1678*	-	501.1680	-	-

[a]All spectra have been internally calibrated using accurate *m/z* values of the parent ion, $(TMPP\text{-}ac\text{-}peptide)^+$ and Ar_3PH^+ ions. Theoretical accurate *m/z* values are given as italics.
[b]Ar = 2,4,6-trimethoxyphenyl

Table 2. ECD Spectra of $(TMPP\text{-}ac\text{-}peptide\text{-}ac\text{-}TMPP)^{2+}$ Ions.

	Peptide			
Ions[a]	GK	KG	AK	KA
M^{2+}	$\mathbf{6}^{2+}$	$\mathbf{7}^{2+}$	$\mathbf{8}^{2+}$	$\mathbf{9}^{2+}$
	674.7526	674.7527	681.7606	681.7603
	674.7525[a]		*681.7603*	
M^{+}	-	-	-	-
$(M - Ar)^{+}$[b]	1182.4343	1182.4345	1196.4503	1196.4497
	1182.4341		*1196.4497*	
$(M - Ar_3P)^{+}$	817.3185	817.3181	831.3336	831.3343
	817.3187		*831.3343*	
$(M - Ar_3P - CH_3O)^{+}$	786.3006	786.2997	800.3171	800.3165
	786.3003		*800.3159*	
$(M - Ar_3P - CH_2CONH(CH_2)_4)^{+}$	704.2316	704.2339	-	718.2508
	704.2346			*718.2503*
$Ar_3P^{+}CH_2CONH(CH_2)_4$	644.2611	644.2623	-	644.2624
	644.2625			

[a]All spectra have been internally calibrated using the accurate *m/z* values of the parent ion, $(M - Ar)^{+}$, and $(M - Ar_3P)^{+}$ fragment ions. Calculated *m/z* values in italics.
[b]Ar = 2,4,6-trimethoxyphenyl.

Table 3. Calculated Ion-Electron Recombination Energies.

Species	Recombination Energy[a] B3LYP 6-311++G(2d,p)	PMP2	B3-PMP2	
PH_4^+	5.92	5.47	5.70	(5.70)[b]
Ph_3PH^+	4.10	4.88	4.49	
$Ph_3PCH_3^+$	3.82	3.50	3.66	
$Ph_3PCH_2CONH_2$	3.85			
Ar_3PH^+ [c]	3.15			
$Ar_3PCH_2CONH_2^+$ [c]	3.07			
$(GK + H)^+$	4.37[d] (3.30)[e]	4.12[d] (3.00)[e]	4.24[d] (3.15[e]	
$(GR + H)^+$	3.87 (2.98)[e]	3.63 (2.64)[e]	3.75 (2.81)[e]	
$(GGK + 2H)^{2+}$	5.76 (5.31)[e]	5.16 (4.56)[e]	5.46 (4.94)[e]	

[a]Adiabatic energies (absolute values) in electron volts including B3LYP/6-31+G(d,p) zero-point energy corrections. [b]Reference adiabatic recombination energy from single-point CCSD(T)/aug-cc-pVTZ calculations. [c]Ar = 2,4,6-trihydroxyphenyl (THPP). [d]Including radical rearrangement in the lysine residue by H atom migration onto the COOH group. [e]Vertical recombination energies.

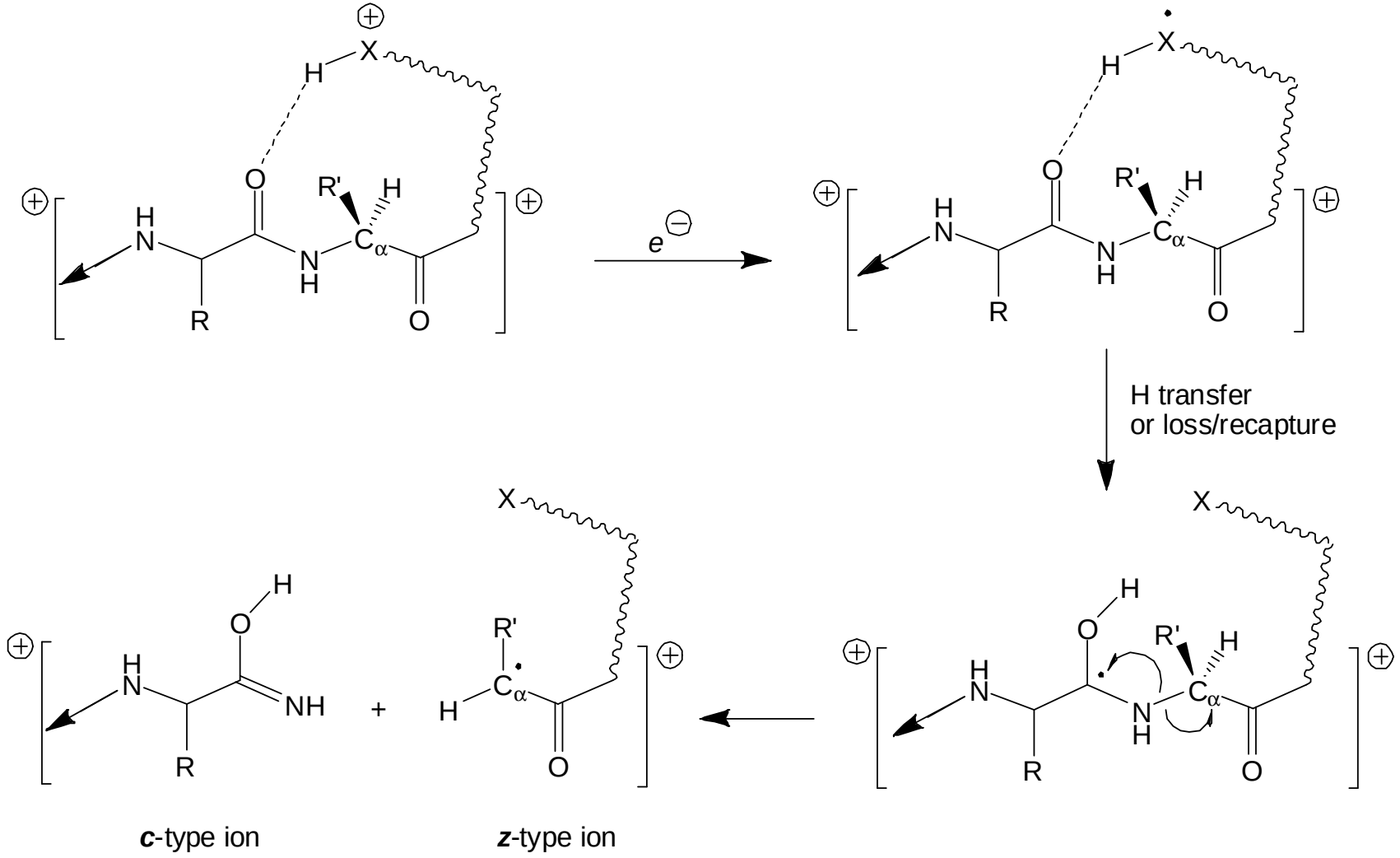

Scheme 1

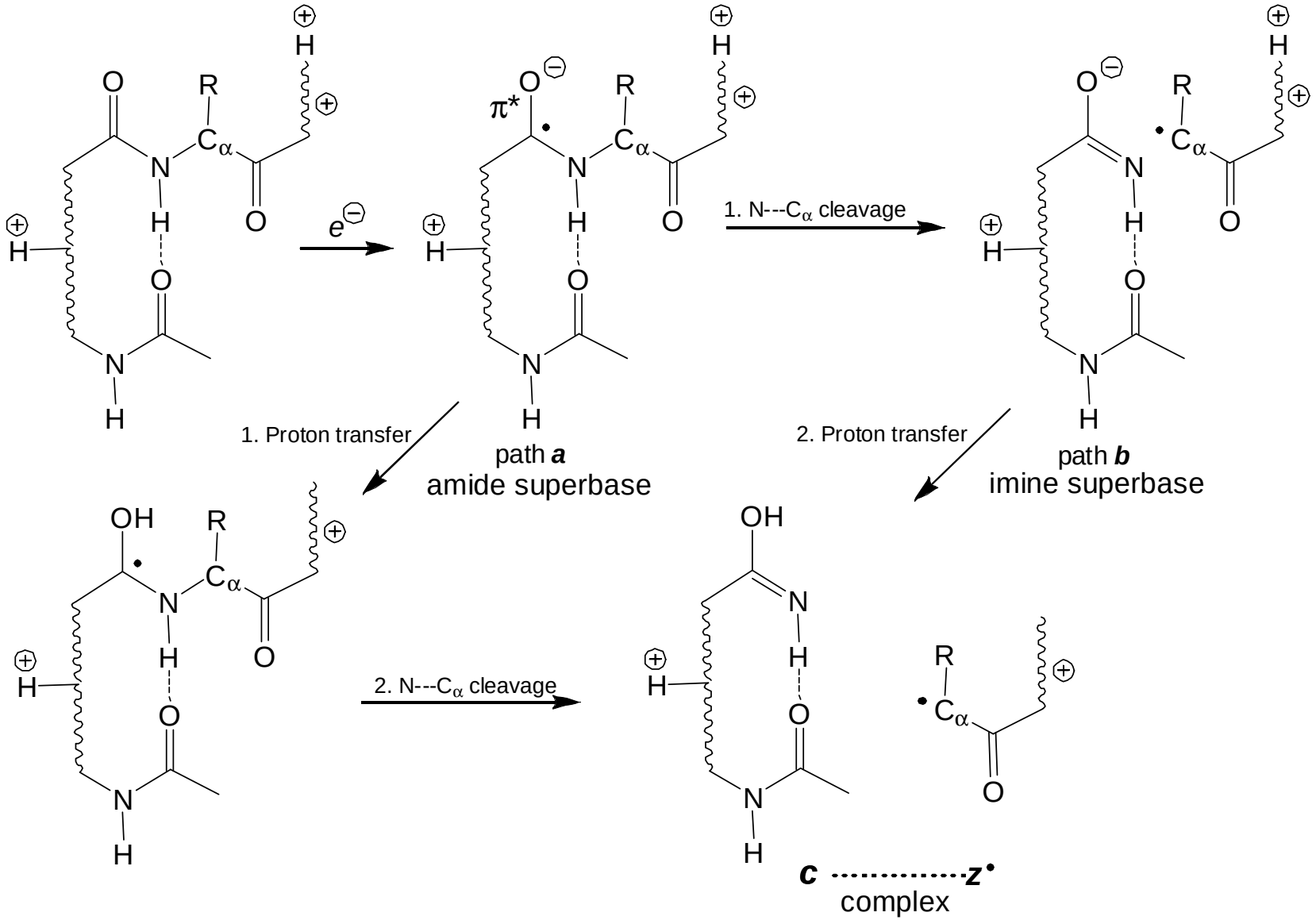
e⊖
1. N---Cα cleavage
1. Proton transfer
path a
amide superbase
2. Proton transfer
path b
imine superbase
2. N---Cα cleavage
c ·····z•
complex

Scheme 2

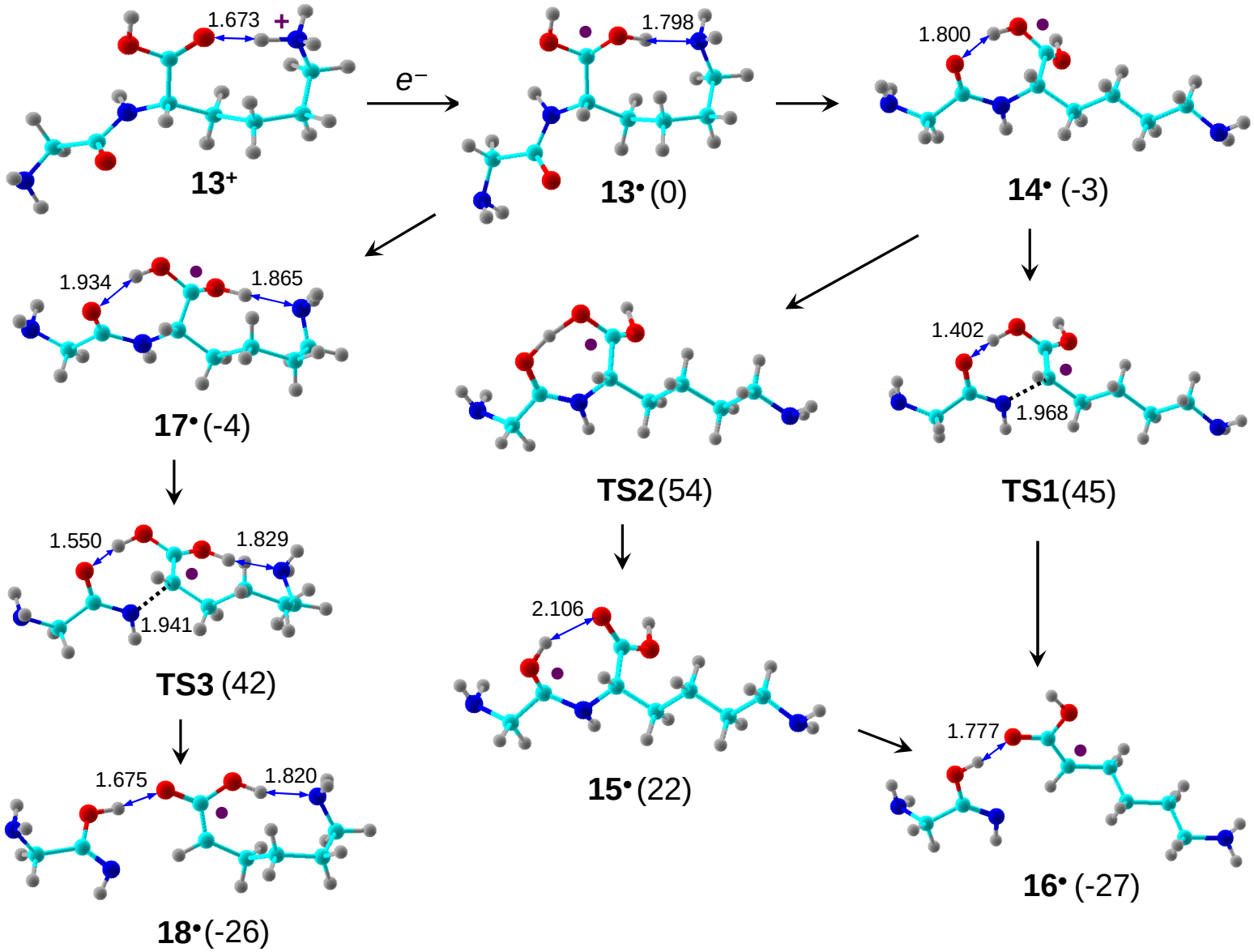
1.673
+
13+
e−
1.798
13• (0)
1.800
14• (-3)
1.934
1.865
17• (-4)
TS2 (54)
1.402
1.968
TS1 (45)
1.550
1.829
1.941
TS3 (42)
2.106
15• (22)
1.777
16• (-27)
1.675
1.820
18• (-26)

Scheme 3

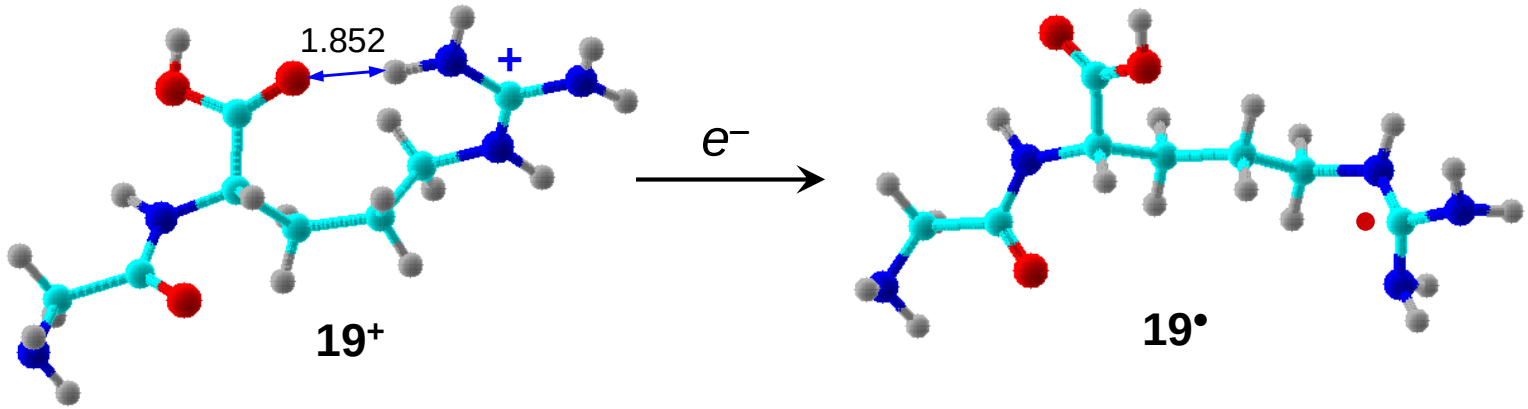

Scheme 4

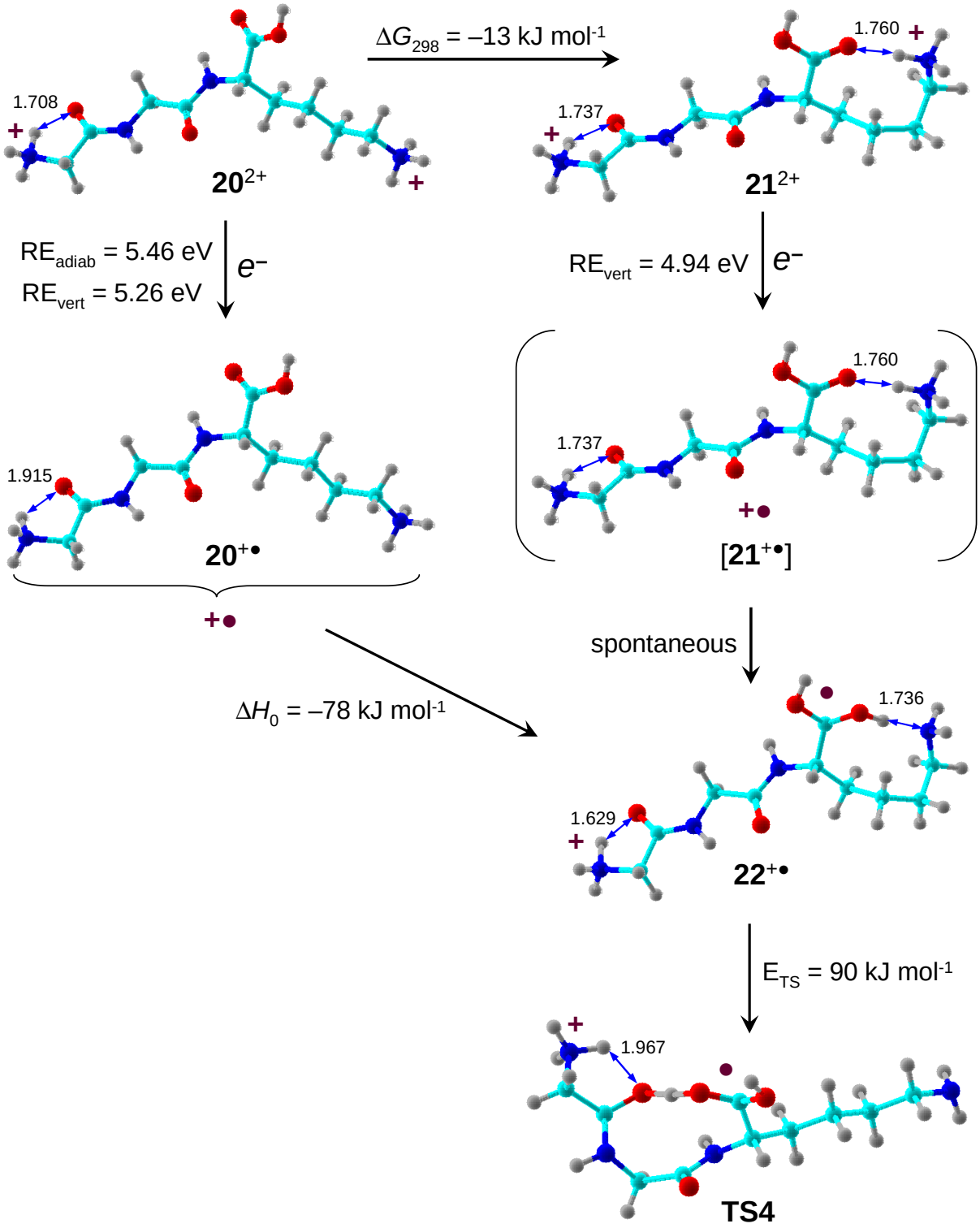
ΔG298 = –13 kJ mol-1
1.708
1.760
1.737
20 2+
21 2+
REadiab = 5.46 eV
REvert = 5.26 eV
e–
REvert = 4.94 eV
e–
1.915
1.760
1.737
20 +•
[21 +•]
+•
spontaneous
ΔH0 = –78 kJ mol-1
1.736
1.629
22 +•
ETS = 90 kJ mol-1
1.967
TS4

Scheme 5

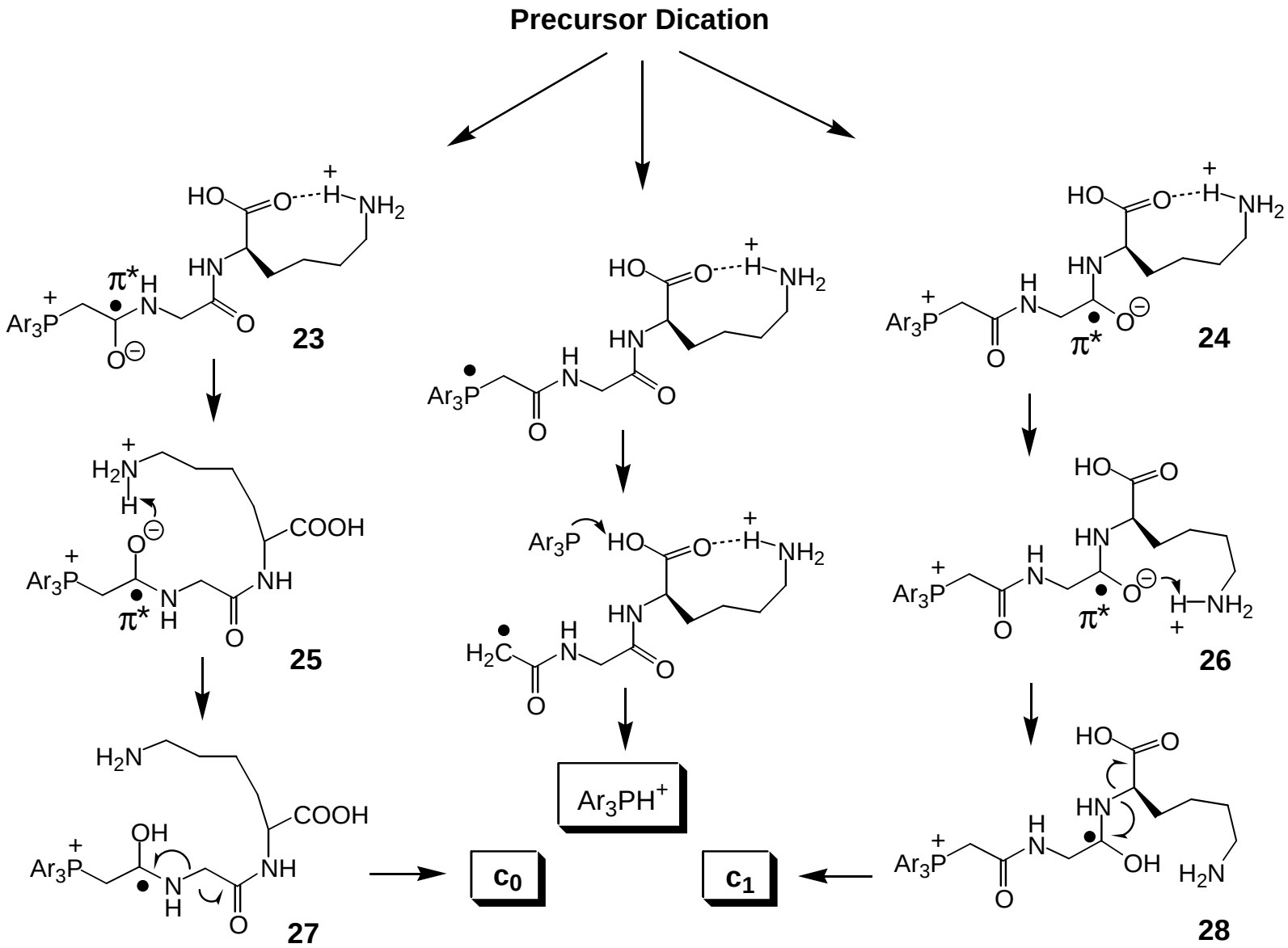

Scheme 6

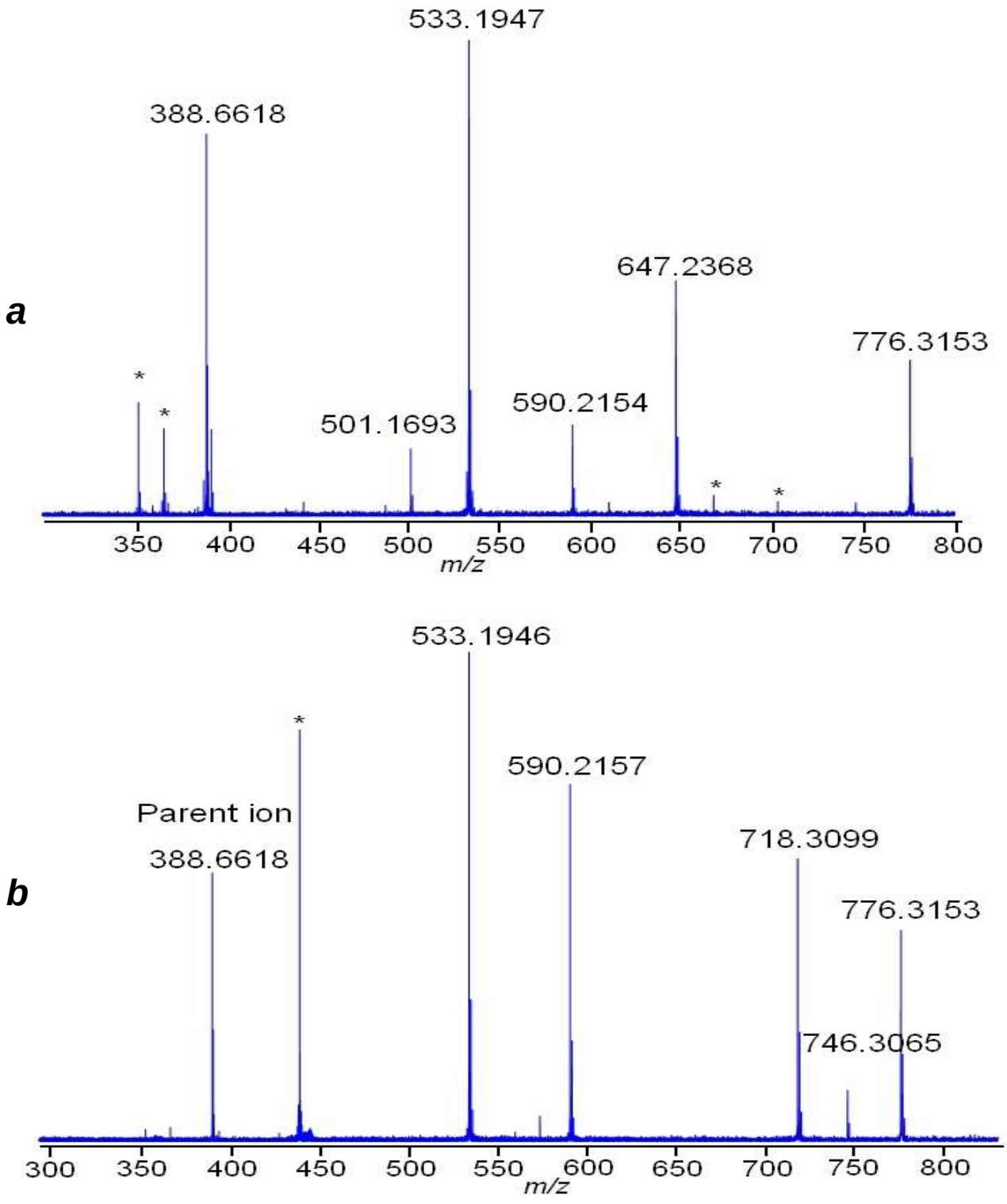
a
533.1947
388.6618
647.2368
776.3153
590.2154
501.1693
*
*
*
*
350
400
450
500
550
600
650
700
750
800
m/z
b
533.1946
*
590.2157
Parent ion
388.6618
718.3099
776.3153
746.3065
300
350
400
450
500
550
600
650
700
750
800
m/z

Figure 1

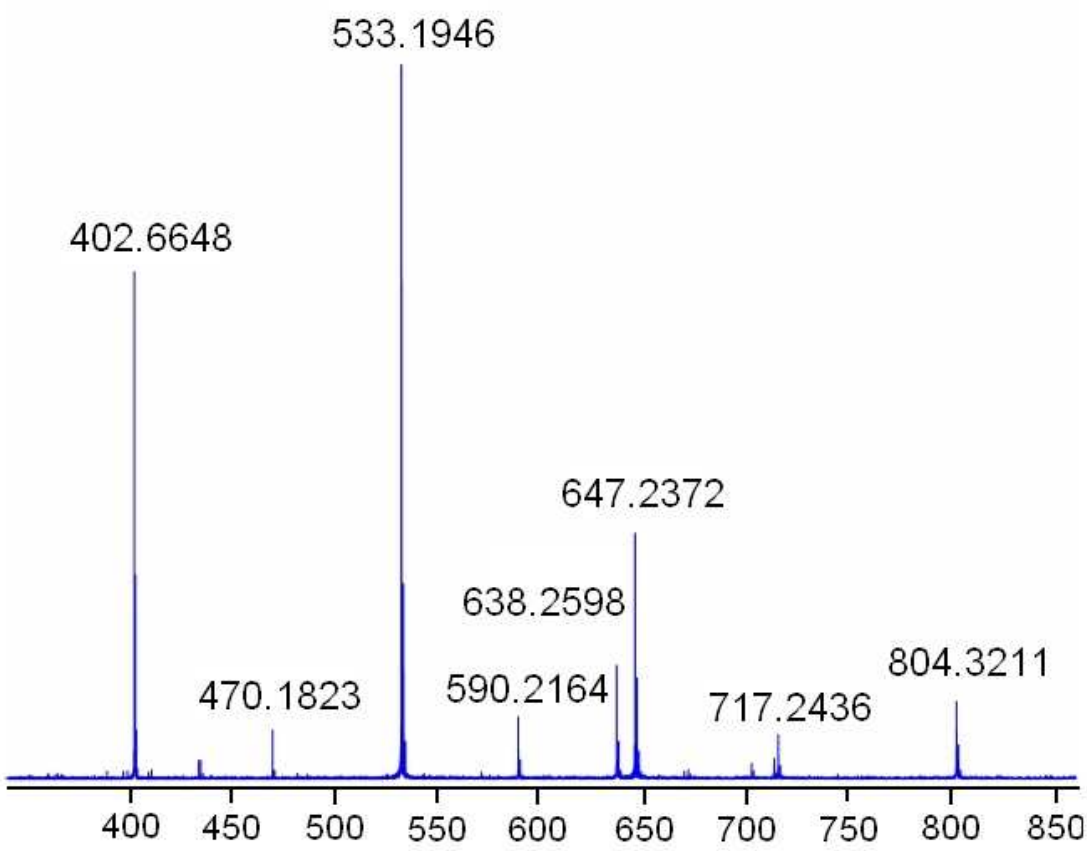
533.1946
402.6648
647.2372
638.2598
804.3211
470.1823
590.2164
717.2436
400
450
500
550
600
650
700
750
800
850

Figure 2

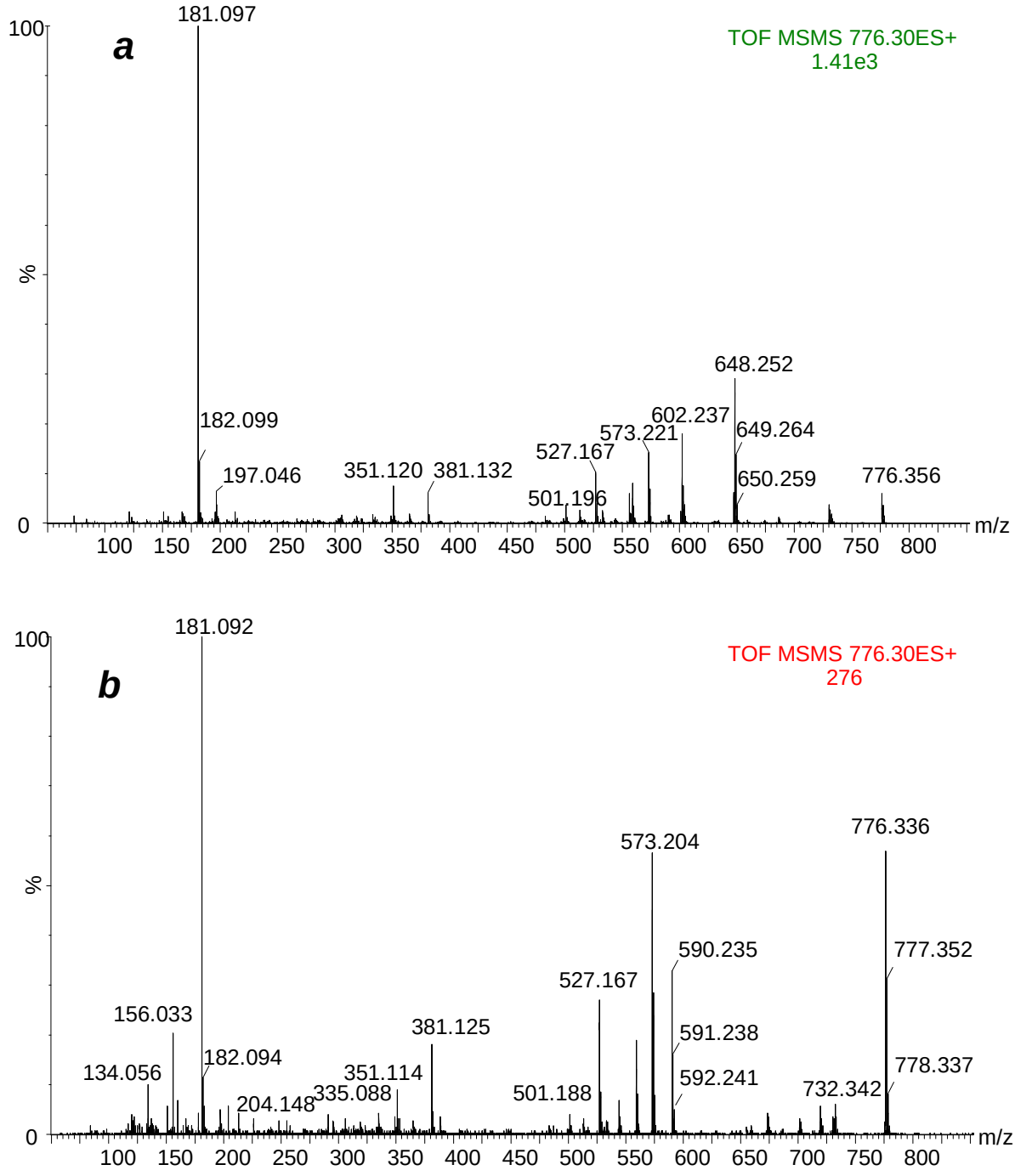
a
TOF MSMS 776.30ES+
1.41e3
100
%
0
181.097
182.099
197.046
351.120
381.132
501.196
527.167
573.221
602.237
648.252
649.264
650.259
776.356
m/z
100 150 200 250 300 350 400 450 500 550 600 650 700 750 800
b
TOF MSMS 776.30ES+
276
100
%
0
181.092
134.056
156.033
182.094
204.148
335.088
351.114
381.125
501.188
527.167
573.204
590.235
591.238
592.241
732.342
776.336
777.352
778.337
m/z
100 150 200 250 300 350 400 450 500 550 600 650 700 750 800

Figure 3

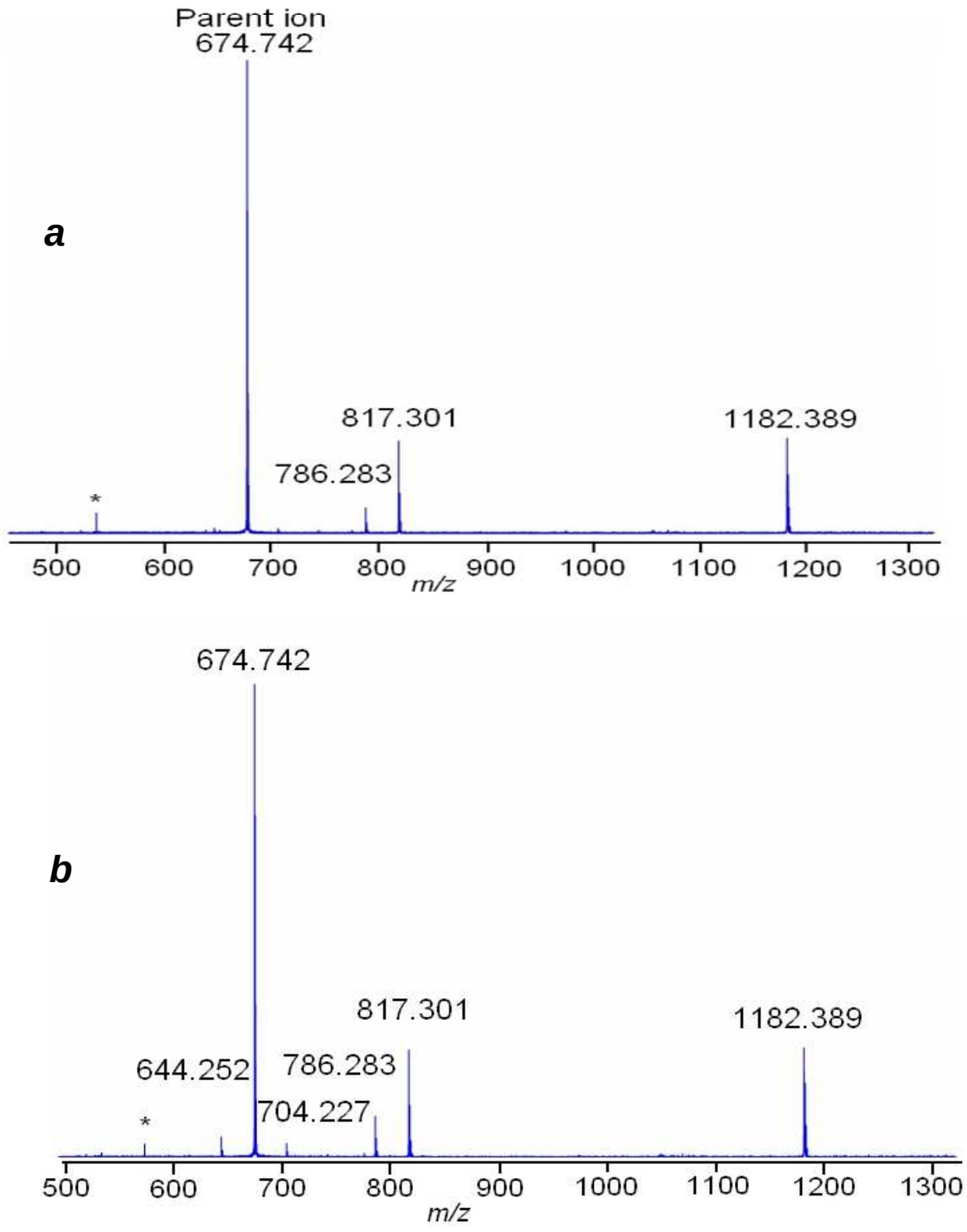
Parent ion
674.742
a
817.301
1182.389
786.283
*
500
600
700
800
900
1000
1100
1200
1300
m/z
674.742
b
817.301
1182.389
644.252
786.283
704.227
*
500
600
700
800
900
1000
1100
1200
1300
m/z

Figure 4

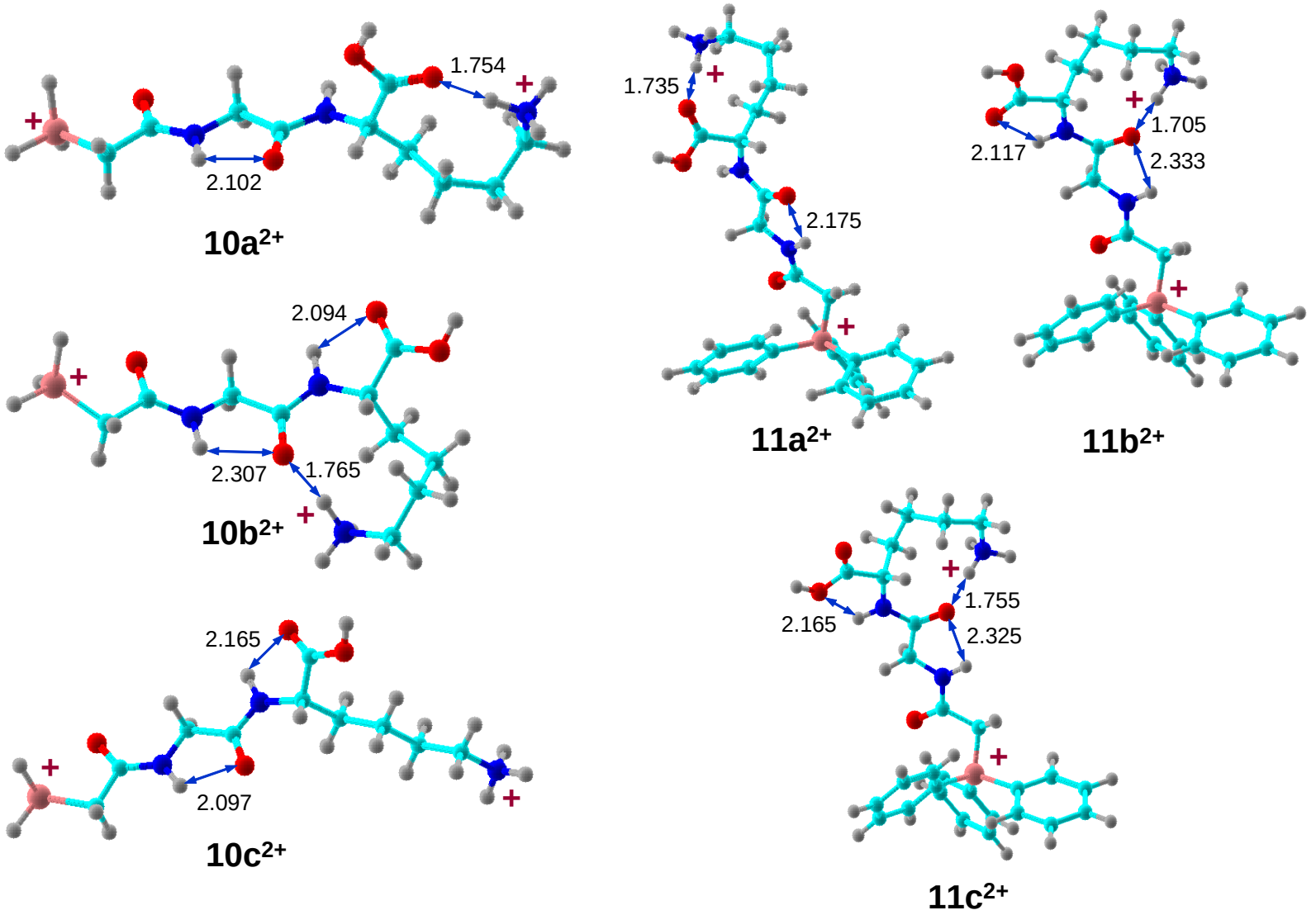
1.754
2.102
10a2+
2.094
2.307
1.765
10b2+
2.165
2.097
10c2+
1.735
2.175
11a2+
1.705
2.117
2.333
11b2+
1.755
2.165
2.325
11c2+

Figure 5

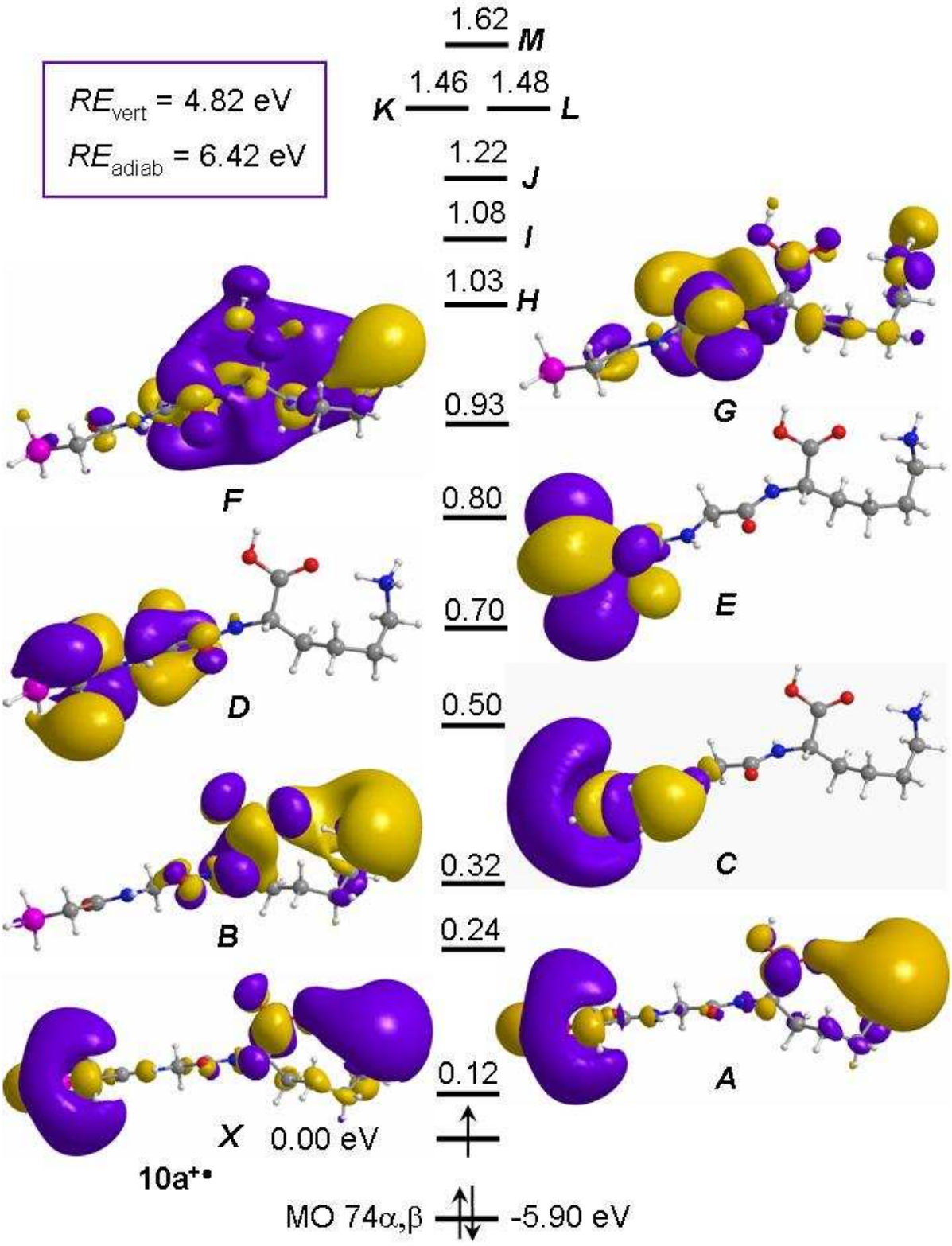
RE_{vert} = 4.82 eV
RE_{adiab} = 6.42 eV
1.62 M
K 1.46 1.48 L
1.22 J
1.08 I
1.03 H
0.93
0.80
0.70
0.50
0.32
0.24
0.12
F
G
E
D
C
B
A
X 0.00 eV
10a+•
MO 74α,β -5.90 eV

Figure 6